Transcytosis of Listeria monocytogenes across the intestinal barrier upon specific targeting of goblet cell accessible E-cadherin

Georgios Nikitas, Chantal Deschamps, Olivier Disson, Théodora Niault, Pascale Cossart, Marc Lecuit

Transcytosis of *Listeria monocytogenes* across the intestinal barrier upon specific targeting of goblet cell accessible E-cadherin

Georgios Nikitas,[1,4] Chantal Deschamps,[1,4] Olivier Disson,[1,4] Théodora Niault,[1,4] Pascale Cossart,[2,5] and Marc Lecuit[1,3,4,6]

[1]Microbes and Host Barriers Group, [2]Bacteria Cells Interactions Unit, and [3]French National Reference Center and World Health Organization Collaborating Center on *Listeria*, Institut Pasteur, F-75015 Paris, France
[4]Institut National de la Santé et de la Recherche Médicale (INSERM) Avenir Unité 604, F-75015 Paris, France
[5]INSERM Unité 604, Institut National de la Recherche Agronomique USC2020, F-75015 Paris, France
[6]Service des Maladies Infectieuses et Tropicales, Centre d'Infectiologie Necker-Pasteur, Hôpital Necker-Enfants Malades, Sorbonne Paris Cité, Université Paris Descartes, F-75015 Paris, France

***Listeria monocytogenes* (*Lm*) is a foodborne pathogen that crosses the intestinal barrier upon interaction between its surface protein InlA and its species-specific host receptor E-cadherin (Ecad). Ecad, the key constituent of adherens junctions, is typically situated below tight junctions and therefore considered inaccessible from the intestinal lumen. In this study, we investigated how *Lm* specifically targets its receptor on intestinal villi and crosses the intestinal epithelium to disseminate systemically. We demonstrate that Ecad is luminally accessible around mucus-expelling goblet cells (GCs), around extruding enterocytes at the tip and lateral sides of villi, and in villus epithelial folds. We show that upon preferential adherence to accessible Ecad on GCs, *Lm* is internalized, rapidly transcytosed across the intestinal epithelium, and released in the lamina propria by exocytosis from where it disseminates systemically. Together, these results show that *Lm* exploits intrinsic tissue heterogeneity to access its receptor and reveal transcytosis as a novel and unanticipated pathway that is hijacked by *Lm* to breach the intestinal epithelium and cause systemic infection.**

CORRESPONDENCE
Marc Lecuit:
marc.lecuit@pasteur.fr

Abbreviation used: AGC, cell away from GCs; Ecad, E-cadherin; GC, goblet cell; hEcad, human Ecad; IEC, intestinal epithelial cell; ITF, intestinal trefoil factor; *Li*, *Listeria innocua*; LLO, listeriolysin O; *Lm*, *Listeria monocytogenes*; mEcad, mouse Ecad; NGC, cell next to GCs; NSF, *N*-ethylmaleimide–sensitive factor; p.i., postinoculation; TEM, transmission electron microscopy; TJ, tight junction; WGA, wheat germ agglutinin.

The interaction of the *Listeria monocytogenes* (*Lm*) surface protein InlA with its receptor E-cadherin (Ecad), expressed by intestinal epithelial cells (IECs), is critical for the translocation of this human foodborne pathogen across the intestinal barrier and the onset of a systemic infection (Lecuit et al., 2001). InlA interaction with Ecad is species specific: human Ecad (hEcad) is a receptor for InlA, whereas mouse Ecad (mEcad) is not (Lecuit et al., 1999). We have shown that in hosts permissive to InlA–Ecad interaction, such as transgenic mice expressing hEcad and knockin mice expressing humanized mEcad, *Lm* directly invades enterocytes and crosses the intestinal epithelium (Lecuit et al., 2001; Disson et al., 2008). However, Ecad is an adherens junction protein typically located below tight junctions (TJs) and is therefore thought to be inaccessible to bacteria located in the intestinal lumen (Boller et al., 1985; Sousa et al., 2005). *Lm* has been reported to invade the tip of intestinal villi at sites of cell extrusion (Pentecost et al., 2006, 2010). An in vitro study in cultured epithelial kidney cells (MDCK cells) has shown that cell extrusion is associated with junction remodeling that transiently exposes Ecad on extruding cells and their immediate neighbors (Pentecost et al., 2006), and in vivo studies have confirmed that this process is accompanied by redistribution of apical junctional complex proteins (Madara, 1990; Marchiando et al., 2011). Nevertheless, apart from intestinal villus tips, the sites of *Lm* adhesion to and translocation across the intestinal epithelium in vivo have not been investigated systematically, and the molecular mechanisms that lead to *Lm* actual

G. Nikitas and C. Deschamps contributed equally to this paper.

The Rockefeller University Press $30.00
J. Exp. Med. Vol. 208 No. 11 2263-2277
www.jem.org/cgi/doi/10.1084/jem.20110560

translocation across the intestinal epithelium and release into the lamina propria remain unknown.

In vitro studies have demonstrated that *Lm* enters into nonphagocytic cells within 10 min through a zippering process (Mengaud et al., 1996; Cossart and Sansonetti, 2004). Upon internalization, the bacterium is entrapped in a membrane-bound compartment, from which it is able to escape within 10–15 min (Myers et al., 2003; Henry et al., 2006). Vacuolar escape is mediated by the pore-forming activity of the secreted cholesterol-dependent listeriolysin O (LLO; Garcia-del Portillo and Finlay, 1995; Cossart and Sansonetti, 2004). Upon vacuolar lysis, *Lm* reaches the cytosol, in which it can polymerize host actin to form comet tails that propel bacteria intracellularly and form protrusions that allow *Lm* transfer into neighboring cells (see schematic representation in Fig. S6 A). This process is strictly dependent on the listerial surface protein ActA, which is necessary and sufficient on the bacterial side to mediate actin polymerization (Kocks et al., 1992). Actin nucleation around bacteria can be observed within 15 min after vacuolar escape, and *Lm*-containing protrusions can be observed ∼2.5 h upon infection (Tilney et al., 1992).

The goal of our study was to determine comprehensively *Lm* intestinal epithelial target cells and to decipher the mechanisms of *Lm* crossing of the intestinal epithelial barrier in vivo. To identify *Lm* intestinal epithelial target cells, we first studied Ecad luminal accessibility by two-photon and confocal imaging of noninfected whole mount intestinal tissue of humanized transgenic mice permissive to InlA and investigated the sites of InlA–Ecad-dependent bacterial association with the intestinal epithelium. We demonstrate that Ecad is luminally accessible at discrete locations, which are (a) junctions between mucus-secreting goblet cells (GCs) and adjacent enterocytes, (b) extruding enterocytes at the tip of villi, as previously proposed by Pentecost et al. (2006, 2010), but also along their lateral sides, and (c) villus epithelial folds. We show that among GCs, those that have expelled their mucus content are those that typically exhibit luminally accessible junctional Ecad. Importantly, we identify GCs as the *Lm* preferential targets at the intestinal barrier level and establish a positive correlation between the number of GCs and the efficiency of *Lm* intestinal invasion and systemic dissemination. We further show that *Lm* translocation across the intestinal epithelium into the lamina propria mostly occurs below intestinal villus tips, is very rapid and efficient, and is strictly InlA dependent, whereas LLO and ActA play no role in this process. Finally, we show that *Lm* is rapidly transcytosed in a vacuole in a microtubule-dependent manner across enterocytes and egresses from them by exocytosis. *Lm* rapid InlA–Ecad-dependent translocation across the intestinal barrier results in a similarly rapid bacterial systemic dissemination.

Transcytosis is a so far unsuspected infection strategy for *Lm*, which is critical for its rapid and efficient crossing of the intestinal epithelium upon targeting of its receptor Ecad. This study provides, to our knowledge, the first in vivo elucidation of how an enteropathogen translocates across the intestinal epithelium into the lamina propria to cause systemic infection. These results illustrate the critical importance of extending cellular microbiology to three-dimensional tissue systems to understand the pathophysiology of infectious diseases.

RESULTS

Lm rapidly translocates across the intestinal epithelium

To study the early stages of *Lm* intestinal crossing, we inoculated intestinal ligated loops of *iFABP*-hEcad transgenic mice, which express hEcad under the control of the *iFABP* promoter (Lecuit et al., 2001), with *Lm* and imaged whole mount small intestinal tissue by two-photon and confocal microscopy. Noninfected small intestinal tissues immunolabeled for hEcad display a typical epithelial honeycomb-like pattern (Fig. 1 A, Fig. S1 A, and Video 1). In infected intestinal loops, as early as 30 min postinoculation (p.i.), bacteria were associated with intestinal villi (Fig. 1 B): we detected *Lm* adhering to the apical surface of enterocytes, within enterocytes, and at the basal pole of enterocytes. To our surprise given this early time point, we also detected *Lm* in the lamina propria (Fig. 1 C and Video 2). Because of the classical intracellular cycle of *Lm* and its time frame in vitro, we would have anticipated that *Lm* intestinal translocation in the lamina propria would require at least 45 min to occur. We thus performed a kinetic analysis of *Lm* invasion of the intestinal tissue and studied the contribution of InlA to this process. Using two-photon and confocal imaging, we compared the association of WT *Lm* to that of its Δ*inlA* isogenic mutant with intestinal villi 5, 15, 30, and 45 min p.i. We observed a time- and InlA-dependent *Lm* association to intestinal villi (Fig. 1 D); as early as 15 min p.i., *Lm* was significantly associated with intestinal villi in a strict InlA-dependent manner. We further quantified bacteria located (a) on the villus surface, (b) in epithelial cells, and (c) in the lamina propria, along the villus vertical axis 30 min p.i. We observed that most bacteria were 40–80 µm away from the villus tip and were located in the lamina propria (Fig. 1 E). We conclude that *Lm* translocation across the intestinal barrier into the lamina propria is strictly InlA dependent, occurs all along the villus z axis, and is particularly rapid.

Ecad is accessible from the luminal side of the intestinal epithelium around GCs

Because *Lm* early translocation across the intestinal barrier is InlA–Ecad dependent and occurs along the z axis of intestinal villi, we investigated Ecad accessibility from the luminal side of uninfected intestinal epithelium of *iFABP*-hEcad transgenic mice. We first performed a double staining, in which luminally accessible hEcad was stained before tissue permeabilization and total hEcad was stained after tissue permeabilization with HECD-1, an mAb raised against extracellular domain of hEcad that does not recognize mEcad (Fig. 2 A). Accessible hEcad was observed at the surface of junctional complexes as well as along the lateral sides of the cells (Fig. 2, A and B, insets; Fig. 3 A, B, and D; and Video 3). We next

investigated the precise location of accessible hEcad on villi. We observed that hEcad is luminally accessible at the tip of villi (Fig. 2 B, arrow; see other examples in Fig. S4 A, insets; and Video 3), as previously proposed (Pentecost et al., 2006). Importantly, we also detected luminally accessible hEcad at distinct spots along the longitudinal axis of intestinal villi (Fig. 2 B, insets; see other examples in Fig. S4, E and I, insets; and Video 3). Similar results were obtained when total and/or accessible endogenous mEcad was labeled in transgenic and WT C57BL/6 mice with ECCD2, an mAb raised against the extracellular domain of mEcad (Fig. S1, B and C), demonstrating that Ecad accessibility does not result from hEcad transgenic expression.

We next determined the relative number of the IECs that express luminally accessible hEcad and found that ∼2% of total IECs fall into this category. To determine the cell subtypes that express accessible hEcad, we costained intestinal villi for luminally accessible hEcad and wheat germ agglutinin (WGA). WGA specifically binds to sialic acid and *N*-acetylglucosaminyl carbohydrate residues present on the plasma membrane of enterocytes and in mucus of GCs (Fischer et al., 1984; Jang et al., 2004). We observed that among enterocytes, which were WGA positive (WGA^+), as expected, some expressed luminally accessible hEcad and were identified as either extruding apoptotic cells or cells located within intestinal epithelial folds (Fig. 2 B, arrow; Fig. S4, A, E, and I; and Videos 3, 8, and 9). Importantly, we also identified isolated WGA–highly positive cells (WGA^{hi}) expressing luminally accessible hEcad (Fig. 2 B, inset; Fig. 3, A, B, and D; Fig. S1 C; Fig. S3 A; and Videos 3 and 4). These WGA^{hi} cells exhibited a weaker

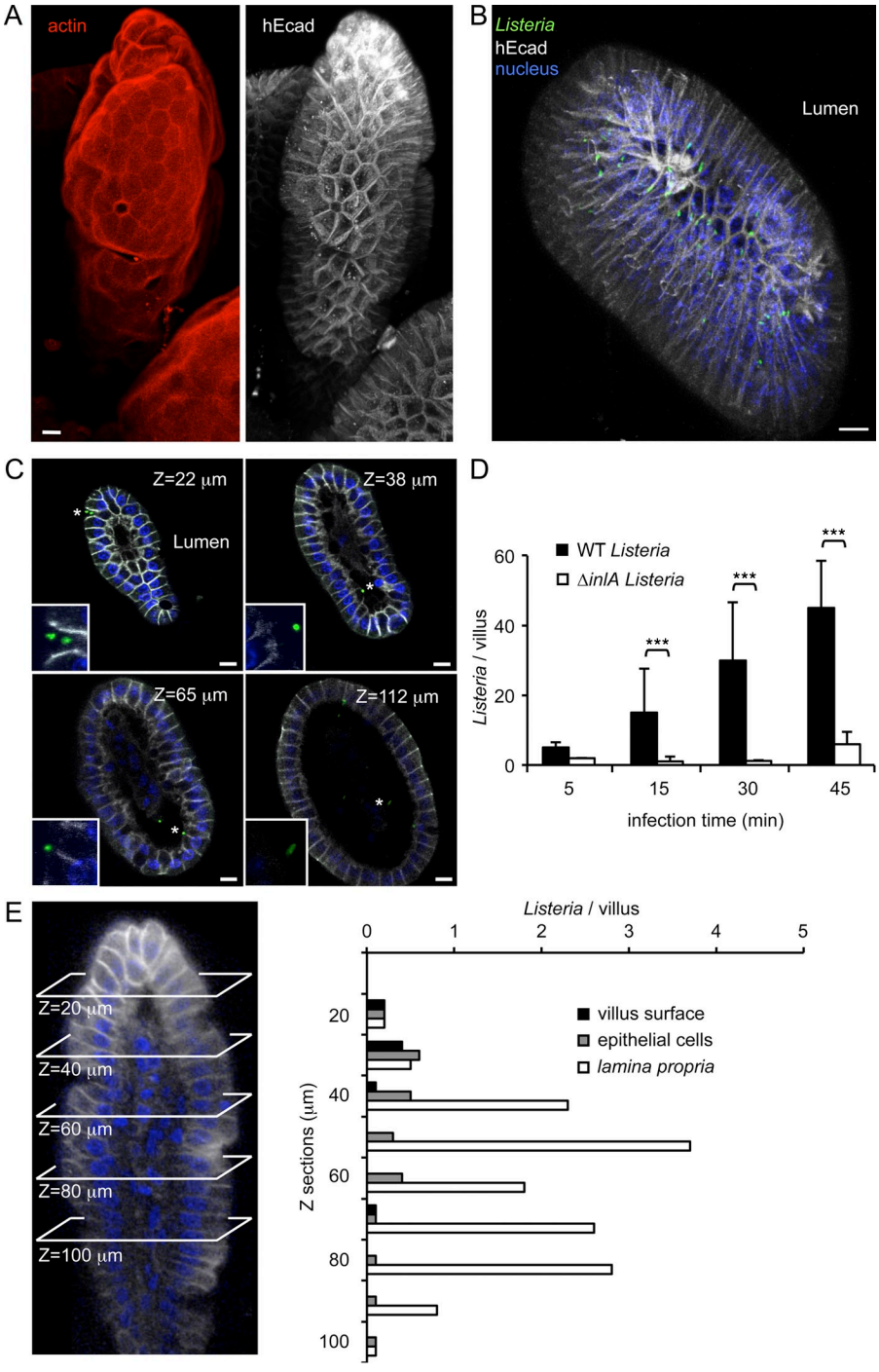

Figure 1. *Lm* rapidly crosses the epithelium of *iFABP*-hEcad transgenic mice in an InlA-dependent manner. (A) Intestinal tissue of *iFABP*-hEcad transgenic mice was fixed, permeabilized, and stained for F-actin and hEcad. A three-dimensional reconstruction of an intestinal villus is shown. (B) Three-dimensional reconstruction of an intestinal villus of *iFABP*-hEcad transgenic mouse infected with 10^9 *Lm* for 45 min and stained for hEcad and nuclei. (C) Optical sections and insets show *Lm* (asterisks) interacting with intestinal villus along its length (z in micrometers corresponds to distance from villus tip). Insets are a magnification of *Lm* (indicated by asterisks) interacting with intestinal villus epithelial cells or inside the lamina propria. Bars, 10 μm. (D) Quantification of *Lm* associated with intestinal villus (***, $P < 0.001$, as assessed by two-way analysis of variance and Tukey adjustment). Error bars indicate SD. $n = 10$ villi from three mice. (E, left) Longitudinal section of a villus on which planes along its z axis are depicted. (right) Quantification of *Lm* localized on the villus surface, in epithelial cells, or in the lamina propria along the z axis of intestinal villi. $n = 10$ villi from three mice. Pictures are representative of three mice.

cortical actin cytoskeleton compared with WGA$^+$ cells (Fig. S2 A, arrows) and were strongly immunolabeled with antibodies against Mucin 2 (Muc-2) and intestinal trefoil factor (ITF; Fig. S2, B and C), identifying them unambiguously as GCs (Poulsom and Wright, 1993; van Klinken et al., 1999). We also observed that hEcad is enriched along the lateral membranes of GCs compared with neighboring enterocytes (Fig. 3 D), whereas accessible hEcad was not detectable at the apical dome of GCs, where Ecad-negative mucin granules fuse with the apical membrane and exocytose their mucus content (Fig. 3, A, B, and D).

We next quantified the relative proportion of GCs and non-GCs that display luminally accessible Ecad: GCs represent 2.8% of the total IECs (Fig. 2, C and D) but account for half of the cells that exhibit accessible hEcad (Fig. 2 E), demonstrating a significant overrepresentation of GCs among cells expressing accessible hEcad; in fact, up to one third of GCs (32%) express luminally accessible hEcad, whereas only a very small proportion (1%) of non-GCs do (Fig. 2 F). Accessible hEcad immunolabeling in the presence of *Lm* was similar to uninfected intestinal tissue (Fig. S2 D), indicating that hEcad luminal accessibility is not induced by *Lm* but rather reflects physiological tissue heterogeneity.

Ecad luminal accessibility on GCs correlates with cell junction reorganization and mucus secretion

Cell–cell junctions involving GCs have been described as heterogeneous and relatively weaker than those between classical enterocytes (Madara et al., 1980; Madara and Trier, 1982). Moreover, cell shape changes that GCs undergo during mucus secretion have been associated with the loosening of their TJs (Hull and Staehelin, 1976; Porvaznik et al., 1983).

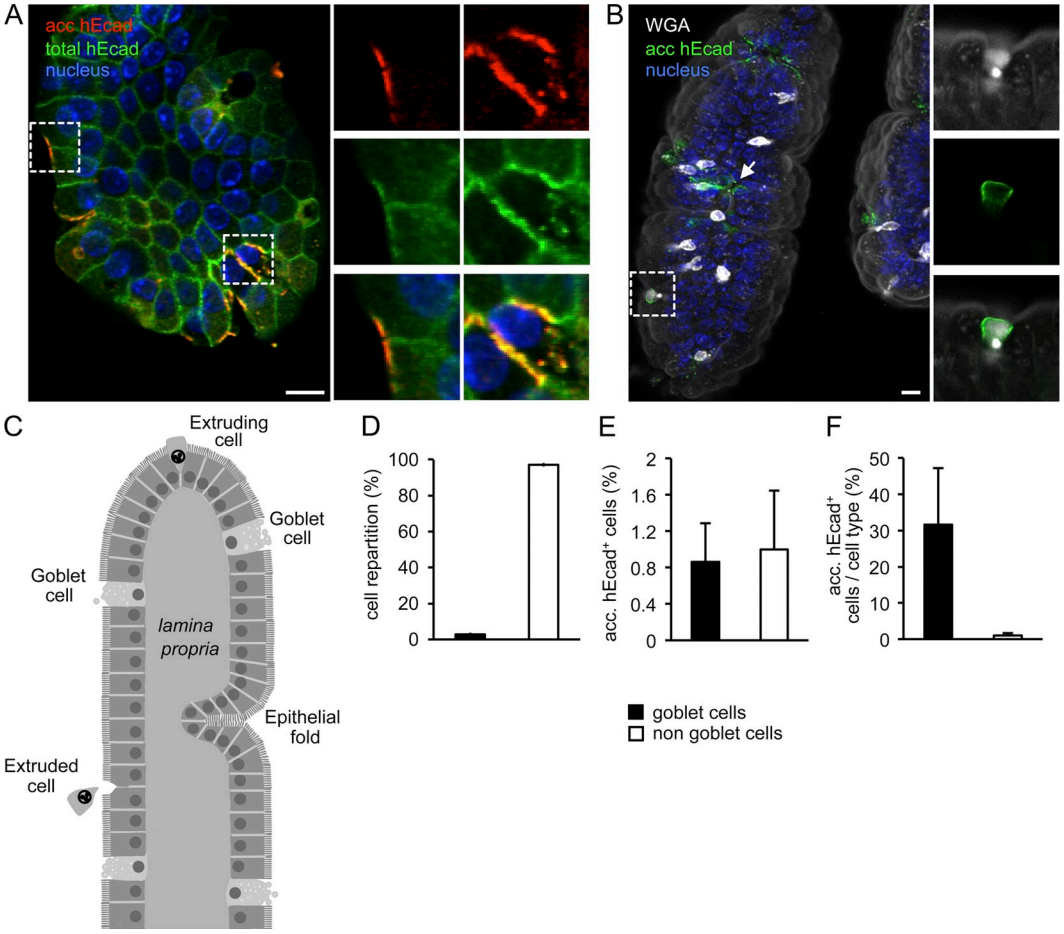

Figure 2. Ecad is accessible from the luminal side of intestinal villi and is mainly detectable around GCs. (A) Intestinal tissue of *iFABP*-hEcad transgenic mice was fixed and stained for luminally accessible (acc) hEcad before tissue permeabilization, total hEcad, and nuclei after tissue permeabilization. The image is an optical section of an intestinal villus. Right panels show separated channels and merge of boxed regions, showing accessible hEcad on the apical and lateral sides of cells. (B) Intestinal cells express luminally accessible hEcad. Stack projection of nonpermeabilized intestinal villi stained with WGA and for accessible hEcad and nuclei. The arrow shows a site of luminally accessible hEcad at the villus tip. Right panels show magnification of the boxed region, which shows a GC surrounded by a ring of accessible hEcad at its apical pole. Pictures are representative of three mice. Bars, 10 µm. (C) Schematic representation of an intestinal villus. (D) Quantification of cell subtypes in intestinal villi. GCs, 2.8%; non-GCs, 97.2%. $n = 20$ villi from two mice. (E) Quantification of cell subtypes expressing luminally accessible hEcad in intestinal villi. $n = 20$ villi from two mice. (F) Relative proportion of cell types with accessible hEcad. $n = 20$ villi from two mice. (D–F) Error bars indicate SD.

To determine whether mucus secretion might provide luminal access to hEcad, we quantified the amount of mucus-expelling GCs that express luminally accessible hEcad. 87% of GCs that express luminally accessible hEcad were secreting or had secreted their mucus content (mucus-expelling GCs; Fig. 3 A). Because TJ disorganization might provide luminal access to hEcad, we investigated their integrity in GCs by studying the localization of two major TJ components, ZO-1 and occludin. In GCs in which hEcad was accessible, both markers exhibited a pattern distinct from classical absorptive epithelial cells, with a thicker occludin signal (Fig. 3 B, Fig. S3 A, and Video 5) and either a thicker ZO-1 signal in cells that had expelled their mucus content (Fig. 3 B) or a fainter signal in cells full of mucus (Fig. S3 B). PKCζ and PAR-3,

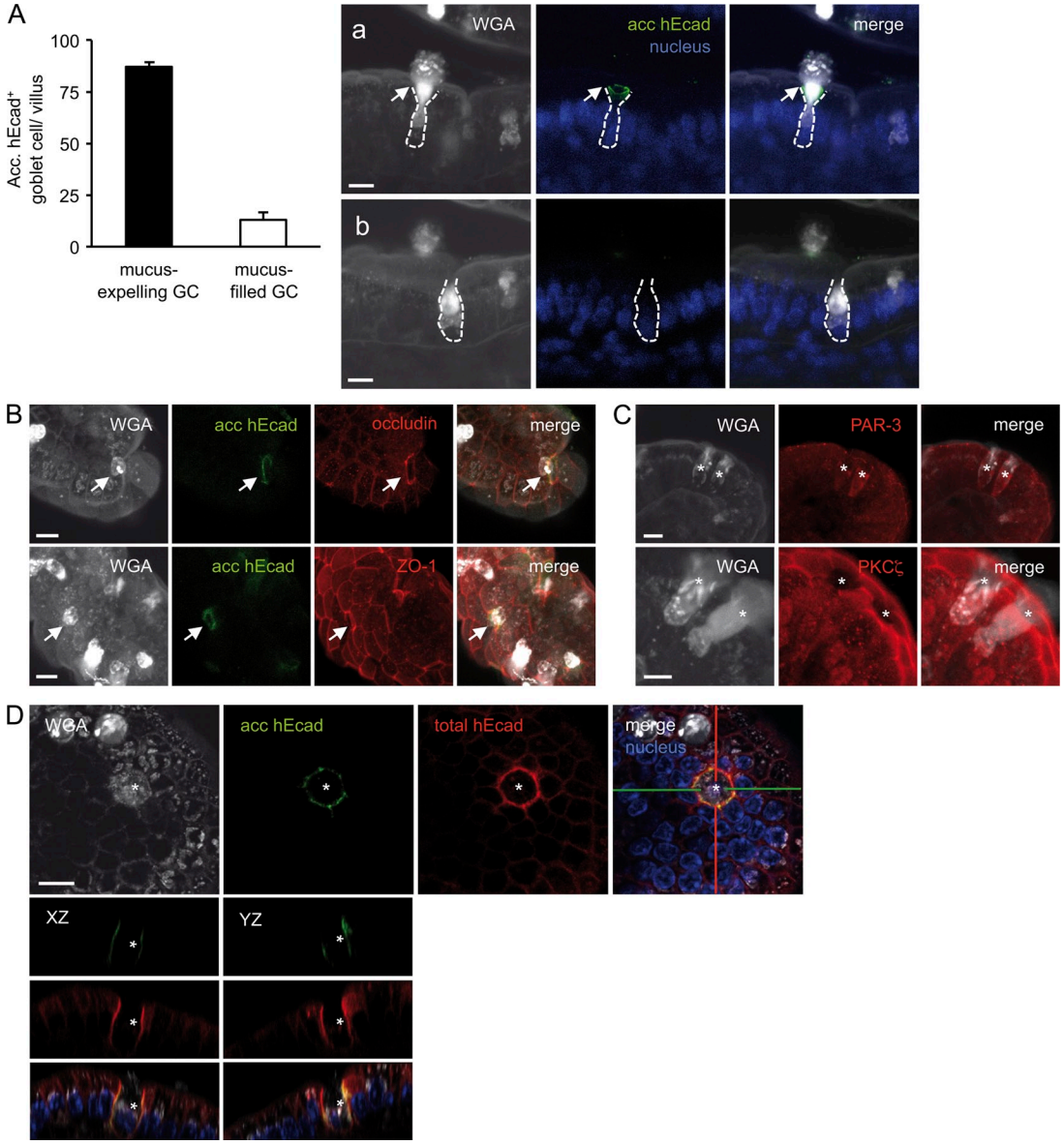

Figure 3. Mucus-expelling GCs exhibit TJ reorganization and delocalization of cell polarity markers and express luminally accessible Ecad. (A) Intestinal tissues were fixed and stained with WGA and for accessible (acc) hEcad and nuclei. Mucus-expelling and mucus-filled GCs expressing luminally accessible hEcad were quantified. Error bars indicate SD. $n = 30$ villi from three mice. (right) Stack projection of intestinal epithelium showing an accessible hEcad$^+$ GC expelling its mucosal content (arrows; a) and an accessible hEcad$^-$ GC full of mucus (b). White dashed lines outline the border of GCs. (B) Intestinal tissues were fixed and stained with WGA and for accessible hEcad and TJ proteins (red). (top) Accessible hEcad of a GC (arrows) colocalizes with thickened TJ protein occludin. (bottom) TJ protein ZO-1 is thickened on the apical side of a GC (arrows) with accessible hEcad. (C, top) PAR-3 is depolarized around mucus-expelling GCs (asterisks). (bottom) PKCζ is delocalized from the apical region on mucus-expelling GCs (asterisks). (B and C) Stack projections of whole mount tissues are shown. (D) Intestinal tissues were fixed and stained with WGA and for accessible hEcad, total hEcad, and nuclei. (top) A GC (asterisks) presents an enrichment of total hEcad along its lateral membranes. (bottom) XZ and YZ sections at selected position. Pictures are representative of three mice. Bars, 10 µm.

together with PAR-6, are known to localize at epithelial junctional complexes and have been implicated in the recruitment of junction proteins at the cell–cell interface and in the establishment and maintenance of cell polarity in *Drosophila melanogaster* and mammalian epithelial cells (Izumi et al., 1998; Ohno, 2001; Hirose et al., 2002). As expected, we observed that PAR-3 and PKCζ were recruited at junctional complexes of absorptive epithelial cells (Fig. 3 C; Fig. S3, C and D; and Videos 6 and 7). In contrast, in GCs, we observed a striking depolarization of PAR-3, which was detectable all along GCs (Fig. 3 C, asterisks; Fig. S3 C; and Video 6), as well as a disappearance of PKCζ accumulation at junctional complexes (Fig. 3 C, Fig. S3 D, and Video 7).

Together, these results indicate that TJs of GCs are disorganized compared with classical TJs on absorptive cells. These structural features of GCs, together with the extensive cell shape changes occurring during mucus secretion, likely account for luminal accessibility of Ecad in mucus-expelling GCs.

As with GCs, non-GCs expressing luminally accessible hEcad exhibited a relative redistribution of TJ proteins and cortical actin network when stained for occludin, ZO-1, and PKCζ (Fig. S4, B–D, F–H, and J–L; and Table S1) and F-actin (Fig. S4 M), respectively. These observations fit with a redistribution of apical junctional complex proteins and an enrichment of Ecad during apoptotic cell shedding at the tip of intestinal villi, as previously shown (Fig. S4, A–H, and N; and Video 8; Marchiando et al., 2011), and with a relative exacerbated tension exerted on cell–cell junctions within villus epithelial folds (Fig. S4, I–L; and Video 9).

Lm preferentially targets intestinal GCs expressing luminally accessible Ecad

Having identified GCs as strongly overrepresented among cells expressing luminally accessible Ecad (Fig. 2 F), we next investigated *Lm* preferential cell targets at the intestinal level. To this end, we distinguished three cell categories: (a) GCs, (b) cells next to GCs (NGCs; i.e., cells forming junctions with GCs), and (c) cells away from GCs (AGCs; i.e., all other IECs; Fig. 4 A).

The relative proportions of GCs, NGCs, and AGCs to total IECs per villus were 2.8%, 8.5%, and 89.5%, respectively (Fig. 4 B). To assess whether *Lm* preferentially targets one cell subtype and to investigate the importance of accessible hEcad in *Lm* association and subsequent translocation, we evaluated the number of WT *Lm* that were associated with each of these three cell categories, in conjunction with the presence of accessible hEcad on these cells and in comparison with the Δ*inlA* *Lm* isogenic mutant. 40 min p.i., we observed that *Lm* adhered to each of these three cell categories expressing accessible hEcad (Fig. 4 A, top) and that *Lm* was translocated from the apical to the basal pole of these three cell categories (Fig. 4 A, middle and bottom). We then determined the preference of *Lm* for each cell type by calculating the number of *Lm* per cell, relative to the respective abundance of each cell type (see Materials and methods). We show that although GCs represent a very low proportion of intestinal cells (2.8%; Fig. 4 B), WT *Lm* interacts >20 times more with GCs than with AGCs (Fig. 4 C, left). In addition, the InlA–Ecad interaction provides a >15-fold *Lm* preference for GCs compared with the Δ*inlA* mutant, which demonstrated no cellular preference (Fig. 4 C, right). Finally, WT *Lm* relative associations per NGC were as low as with AGCs. Overall, these results demonstrate that *Lm* preferentially

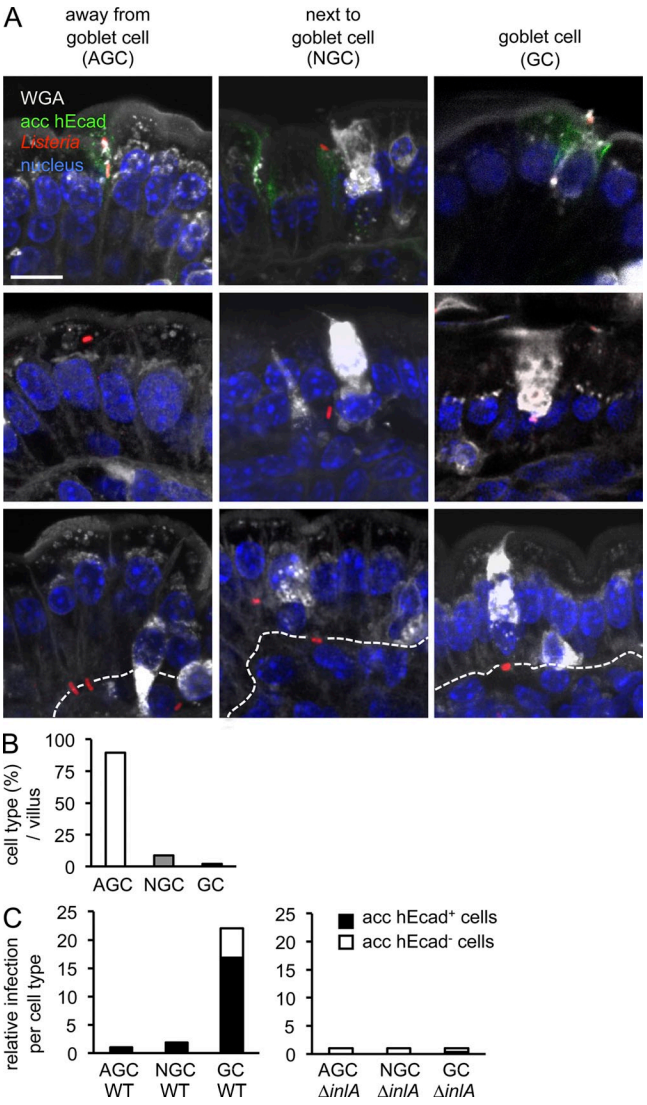

Figure 4. *Lm* interacts preferentially with GCs at sites where hEcad is luminally accessible and transits toward the lamina propria. (A) The intestinal loop of *iFABP*-hEcad transgenic mice was infected with 3×10^9 *Lm* for 40 min. The intestinal tissue was fixed and stained with WGA and for hEcad and nuclei. Optical sections of intestinal mucosa show *Lm* interacting in and entering an IEC away from (left), next to (middle), and in (right) GCs at sites where hEcad is luminally accessible (top). (middle) *Lm* in an IEC. (bottom) *Lm* exits IECs at their basolateral side. Dashed lines indicate basal membrane separating the intestinal epithelium from the lamina propria. Pictures are representative of three mice. Bar, 10 µm. (B) Quantification of cell subtypes per villus. $n = 30$ villi from three mice. (C) Relative infection per cell type: number of *Lm* WT (left) and Δ*inlA* (right) associated with the different cell subtypes expressing or not luminally accessible (acc) hEcad 30 min after infection has been calculated and AGC *Lm* WT set to 1. $n = 12$ villi from two mice.

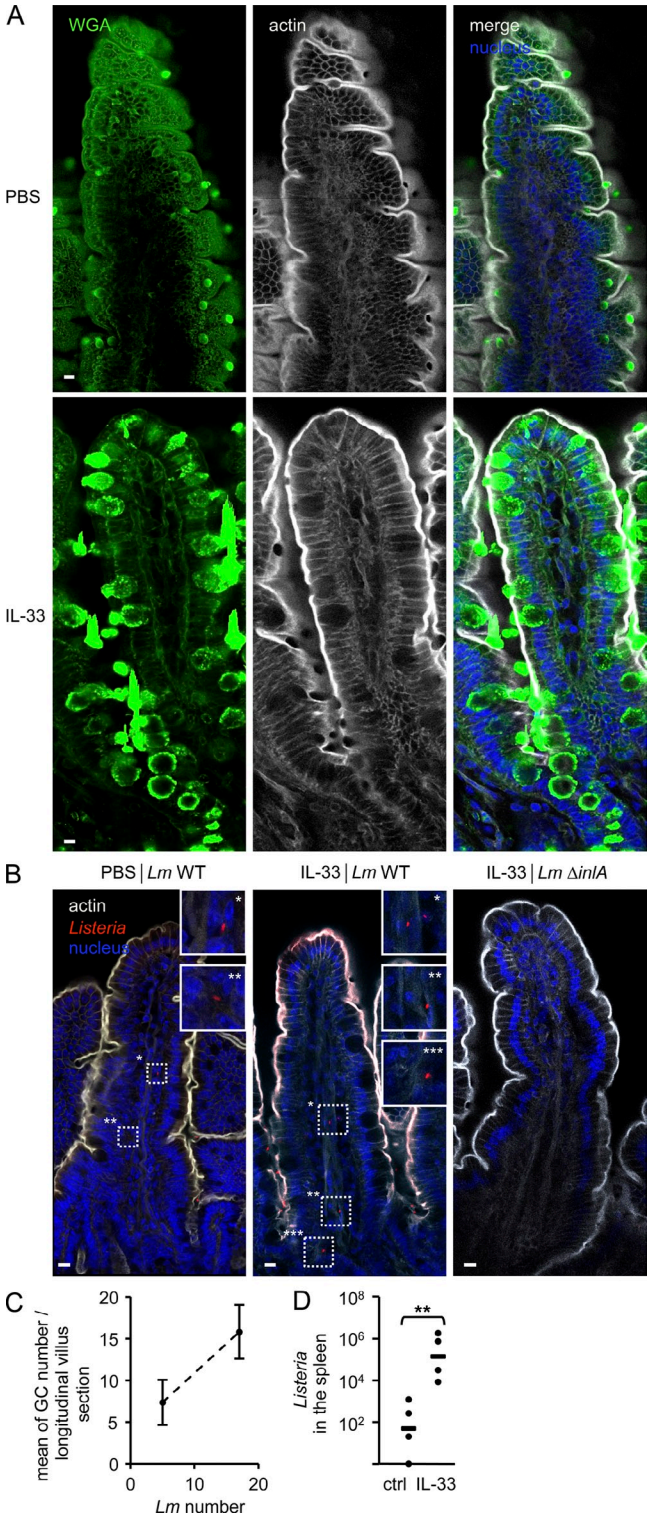

Figure 5. Positive correlation between the number of GCs and the efficiency of *Lm* intestinal invasion and systemic dissemination. IL-33 or PBS alone was administered daily intraperitoneally to *iFABP*-hEcad transgenic mice for 3 d. Imaging and bacterial inoculation were performed on day 3. (A) Optical section of intestinal villus stained with WGA and for F-actin. Intestinal villi of IL-33–treated mice (bottom) exhibit far more GCs, and GCs secrete far more mucus than PBS-treated control mice (top). (B) Inoculation of intestinal ligated loop were performed on day 3 with 3×10^9 of the indicated strain for 45 min. Panels show optical section of intestinal villus after a ligated loop infection of PBS-treated mouse with *Lm* WT, IL-33–treated mouse with *Lm* WT, or IL-33–treated mouse with *Lm* Δ*inlA*. Infected intestinal villi were stained for F-actin, nucleus, and *Lm* (boxes and insets). (A and B) 250-µm vibratome sections are shown. Pictures are representative of two mice. Bars, 10 µm. (C) Quantification of GCs and internalized *Lm* in intestinal villus of PBS- or IL-33–treated mice after a ligated loop infection of 45 min with 3×10^9 *Lm*. For each intestinal villus, GCs were enumerated on the larger longitudinal section of observed villi. Error bars indicate SD. $n = 20$ villi from two mice. (D) Quantification of *Lm* in the spleen after a ligated loop infection of 45 min in PBS- or IL-33–treated mice on day 3. Horizontal bars indicate the mean. $n = 4$ mice (**, $P < 0.01$, as assessed by Student's *t* test).

targets accessible Ecad-expressing GCs on the epithelium of intestinal villi.

To further reinforce the critical role of GCs in *Lm* crossing of the intestinal barrier, we next investigated how variation in the number of GCs would influence *Lm* intestinal tissue invasion and systemic dissemination. We treated hEcad transgenic mice with IL-33, which is well characterized as inducing an increase in the number of GCs and mucus secretion (Moro et al., 2010; Neill et al., 2010). As expected, IL-33–treated mice exhibited an increase in the number of GCs per villus, as well as an increase in the amount of mucus produced (Fig. 5, A and C). Strikingly, this increase in GCs correlated with an increase in *Lm* invasion of intestinal villi (Fig. 5, B and C) and systemic dissemination to the spleen (Fig. 5 D). Increased intestinal invasion was not observed with the Δ*inlA* mutant (Fig. 5 B). Together, these results highlight a positive correlation between the number of GCs and *Lm* intestinal tissue invasiveness and systemic dissemination.

Lm does not need to access the host cell cytosol and polymerize actin to be translocated across the intestinal barrier

Having identified how and where *Lm* interacts with the intestinal barrier in vivo and shown that its transfer into the lamina propria is particularly rapid, we next investigated the molecular mechanisms underlying *Lm* transepithelial translocation. We infected intestinal loops of hEcad transgenic mice with 10^9 *Lm* or an isogenic Δ*inlA* mutant, a Δ*hly* mutant (not expressing LLO), a Δ*actA* mutant, a nonpathogenic and noninvasive *Listeria innocua* (*Li*), or *Li*-expressing InlA (*Li*(*inlA*)). We quantified the amount of bacteria located in the intestinal lamina propria 30 min upon infection. We observed no translocation to the intestinal lamina propria with the Δ*inlA* deletion mutant or, as expected, with the noninvasive *Li* (Fig. 6 A). In contrast, *Li*(*inlA*) translocated rapidly into the lamina propria in equal numbers to *Lm* (Fig. 6 A). Strikingly, the Δ*hly* and Δ*actA* deletion mutants were able to invade and cross the intestinal epithelium as efficiently as WT *Lm*. This demonstrates that the rapid translocation of *Lm* across the intestinal barrier is strictly dependent on the InlA–Ecad interaction, whereas the major virulence factors LLO and ActA are not required (Fig. 6 A), showing that the classical

cell infection cycle of *Lm* is not at play in this process (Fig. S6 A). Furthermore, as early as 30 min p.i., *Lm* disseminated into deeper organs, such as the spleen (Fig. 6 B), in an InlA-dependent but LLO- and ActA-independent manner (Fig. 6 B), clearly demonstrating the significance of the InlA-dependent but LLO- and ActA-independent rapid intestinal translocation for the onset of systemic listeriosis.

Lm transcytoses across IECs and exocytoses at their basal pole

The demonstration that LLO and ActA are dispensable for *Lm* translocation across the intestinal epithelium led us to formulate the hypothesis of a rapid apicobasal transcytosis of *Lm*-containing vacuole and the exocytosis of *Lm* at the basal pole of enterocytes in the lamina propria. We first investigated the role of a critical component of the transcytosis machinery, the microtubule network, in *Lm* translocation across the intestinal barrier using nocodazole, which prevents microtubule polymerization, and colchicine, which leads to dynamic instability and rapid microtubule depolymerization (De Brabander et al., 1976; Lee et al., 1980; Ravelli et al., 2004). Intestinal ligated loops were infected with 10^9 *Lm* for 10 min. Nocodazole or colchicine was then added and left in contact with the bacteria for 50 min. In nocodazole- as well as in colchicine-treated tissues, *Lm* resided within IECs (Fig. 6, C and D). Under these experimental conditions, *Lm* internalization into enterocytes was not affected, and the integrity of adherens junctions and TJs was preserved (Fig. S5 A). Yet microtubule depolymerization inhibited *Lm* translocation across the intestinal epithelium. In fact, in nocodazole- and colchicine-treated loops, the amount of bacteria associated with enterocytes was four times higher than in untreated loops (Fig. 6 C). In contrast, taxol, which inhibits disassembly of microtubules and stabilizes the microtubule network (Schiff and Horwitz, 1980), did not reduce *Lm* rapid translocation (unpublished data).

To investigate the role of vesicle fusion machinery in *Lm* release from its vacuole into the lamina propria, we investigated the contribution of *N*-ethylmaleimide–sensitive factor (NSF) during infection of intestinal ligated loops. We used a fusion polypeptide (TAT-NSF_{700}), composed of an HIV transactivating regulatory

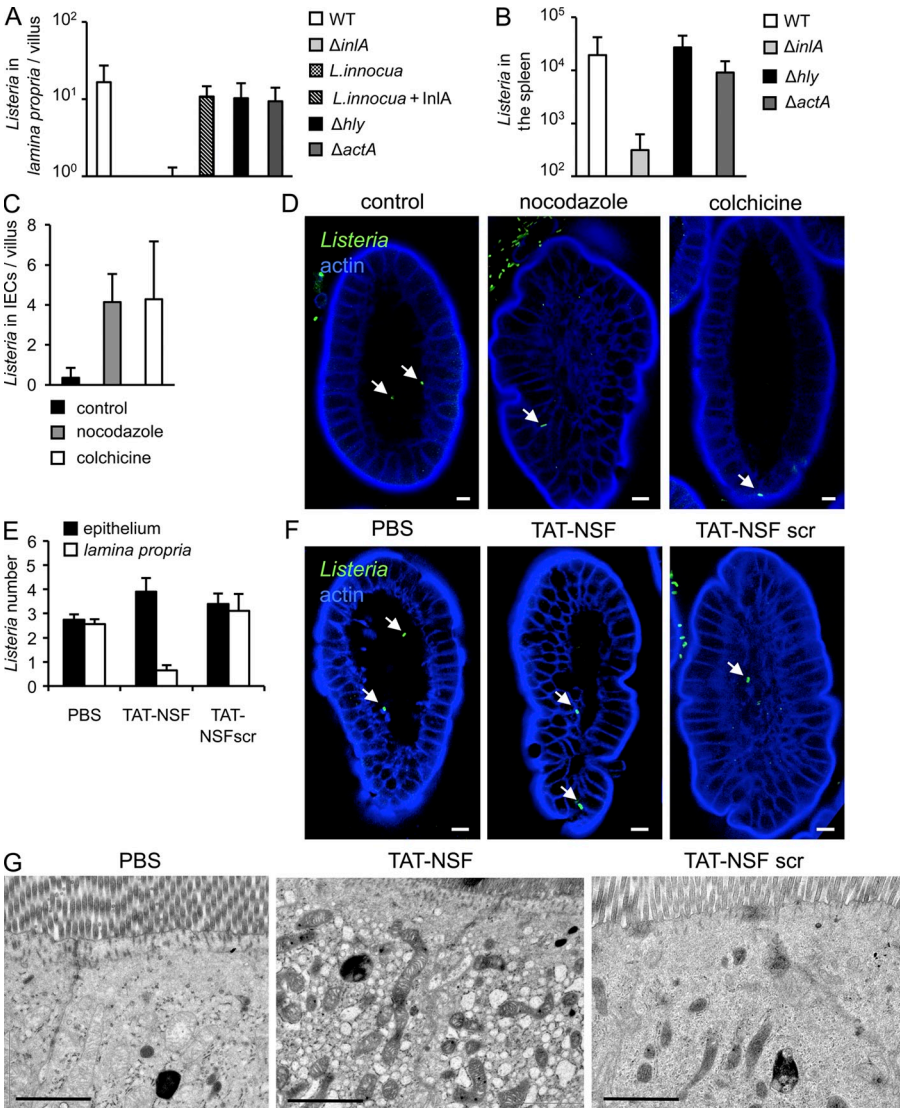

Figure 6. *Lm* translocates through IECs in an InlA-dependent but LLO- and ActA-independent manner. (A) Intestinal loops were infected with 10^9 of the indicated *Listeria* strains, and bacteria were quantified in the lamina propria after 30 min. $n = 30$ villi from three mice. (B) Intestinal loops were infected with the indicated *Listeria* strains, and bacteria were quantified in the spleen after 30 min of infection. $n = 5$ mice. (C) Quantification of *Lm* located in IECs in tissue treated with 10 µg/ml nocodazole, 10 µg/ml colchicine, or their corresponding vehicles (control) for 50 min out of 60 min of *Lm* infection. $n = 11$, 15, and 14 infected villi from three mice, respectively. (D) Optical sections of *Lm*-infected villus treated with PBS as a control, nocodazole, or colchicine for 50 min out of 60 min of *Lm* infection. Arrows points to *Lm* either inside epithelial cells or in the lamina propria. (E) Quantification of *Lm* located in intestinal epithelium or in the lamina propria of tissue treated with PBS (control), 20 µg/ml TAT-NSF_{700}, or 20 µg/ml TAT-NSF scr for 30 min and during *Lm* infection for 45 min. $n = 20$ infected villi from three mice. (A–C and E) Error bars indicate SD. (F) Optical sections of intestinal villus treated with PBS as a control, TAT-NSF peptide, or TAT-NSF scr for 30 min and infected with *Lm* (arrows) in the presence of the peptides for 45 min. (D and F) Tissues are stained for F-actin. Pictures are representative of three mice. (G) TEM sections of PBS-, TAT-NSF_{700}–, or TAT-NSF_{700}scr–treated tissues. Pictures are representative of two mice. Bars: (D and F) 10 µm; (G) 2 µm.

peptide derived from the TAT protein domain fused to a peptide derived from the D2 domain of NSF, which binds ATP and regulates NSF hexamerization. TAT-NSF_{700} has been shown to cross cellular membranes, inhibit NSF hydrolysis of ATP, decrease NSF disassembly of SNARE molecules, and disrupt vacuolar trafficking including exocytosis (Matsushita et al., 2005; Jahn and Scheller, 2006). We pretreated intestinal ligated loops with TAT-NSF_{700} or with a control peptide, TAT-NSF_{700}scr, for 30 min. Entry of TAT-NSF_{700} peptide in intestinal epithelium was verified using a TAT-NSF_{700} peptide conjugated to cyanin 3 (Fig. S5 B). This treatment led to an intracytosolic accumulation of vesicles, which is consistent with the inhibition of the fusion machinery by TAT-NSF in enterocytes (Fig. 6 G). We then injected into the loops 10^9 *Lm* in the presence of each of the synthetic peptides. By two-photon microscopy of whole mount tissue, we determined and quantified *Lm* association with the epithelial sheet and its translocation into the lamina propria 45 min p.i. In TAT-NSF_{700}–treated tissue, *Lm* translocation into the lamina propria was strongly inhibited, and bacteria remained within enterocytes, at the level of their basal pole. In untreated loops and in loops treated with TAT-NSF_{700}scr, bacteria were seen both in the lamina propria and within enterocytes (Fig. 6, E and F). Importantly, entry of *Lm* was not affected by TAT-NSF_{700} treatment because total *Lm* number per villus was not significantly different in PBS-, TAT-NSF_{700}–, or TAT-NSF_{700}scr–treated tissue. Finally, by using transmission electron microscopy (TEM), we observed *Lm* enclosed in a vacuole below the cell nucleus of an IEC and in the vicinity of its basal pole in a TAT-NSF–treated tissue (Fig. 7 C). Together, these results

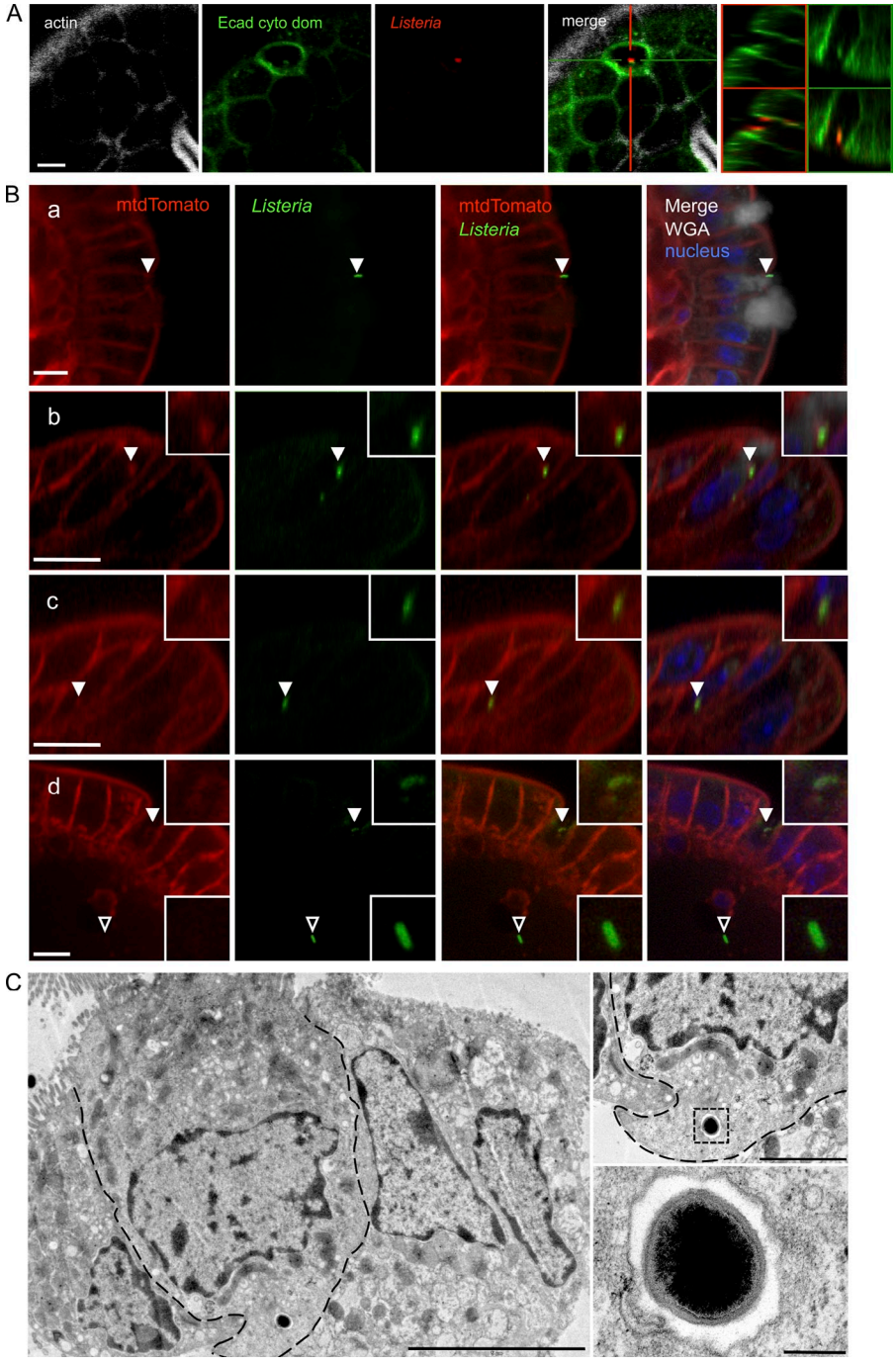

Figure 7. *Lm*–containing vacuole transfer across the intestinal barrier. (A) Intestinal tissue of *iFABP*-hEcad transgenic mice was infected with 10^9 *Lm* for 45 min, fixed, and stained for F-actin, Ecad cytoplasmic domain (cyto dom), and *Lm*. XZ and YZ show sections at selected positions. (B) Optical sections of infected intestinal villi of mtd Tomato mouse stained for *Lm* and nuclei and with WGA. (a) *Lm* (arrowheads) interacting with and entering an enterocyte. (b and c) *Lm* (arrowheads, insets) inside an enterocyte and associated with membrane (red). (d) *Lm* (open arrowheads, bottom insets) in the lamina propria and not associated with membrane and another *Lm* (closed arrowheads, top insets) inside an enterocyte and associated with membrane (red). (C) TEM sections of TAT-NSF–treated and 45-min *Lm*-inoculated ligated loop. (left) Intracellular *Lm* located below the cell nucleus and close to the cell membrane (dashed black line) of an IEC. (top right) Higher magnification of main panel. Intracytosolic *Lm* is located close to the basal cell membrane (dashed black line). (bottom right) Higher magnification of top right panel (boxed area). Intracytosolic *Lm* is enclosed in a membrane vacuole. Pictures are representative of two mice. Bars: (A and B) 10 µm; (C, left) 5 µm; (C, top right) 2 µm; (C, bottom right) 200 nm.

show that disruption of vacuolar trafficking including exocytosis impairs *Lm* translocation into the lamina propria.

We next attempted to colocalize translocating *Lm* with its surrounding membrane vacuole. We first used an antibody raised against the cytoplasmic domain of Ecad, which is expected to decorate the cytoplasmic side of *Lm*-containing vacuole. We observed *Lm* colocalizing with the cytoplasmic domain of Ecad (Fig. 7 A). To directly visualize vacuolar membrane around *Lm*, we crossed our mice expressing humanized Ecad with a transgenic mouse line expressing a membrane-targeted Tomato protein (mtd Tomato), in which all membranes are constitutively fluorescently labeled in red (Disson et al., 2008; Muzumdar et al., 2007). Infection of hEcad × mtd Tomato mice allowed the visualization of red membranes surrounding *Lm* during its apicobasal translocation, whereas *Lm* was no longer associated with a red signal once released in lamina propria (Fig. 7 B). These data confirm that *Lm* is transferred in the lamina propria in a membrane-bound vacuole. Collectively, these results show that *Lm* is transferred apicobasally in a microtubule-dependent manner, is enclosed in a membrane-bound vacuole, and egresses the cell by exocytosis. This process can thus be referred to as transcytosis.

DISCUSSION

Microbial crossing of host barriers is a critical step of invasive infections. Understanding how microbes cross the intestinal barrier is thus key to comprehend the pathophysiology of foodborne infections. *Lm* is a model microorganism for which a great deal of knowledge has been obtained by combining in vitro and in vivo approaches. Yet how this foodborne pathogen actually crosses the intestinal barrier has remained elusive. Pentecost et al. (2006, 2010) have reported that *Lm* targets intestinal villus tips to invade the epithelium at sites of cell extrusion and, based on in vitro observation obtained in cultured kidney epithelial cells, proposed that these were sites of accessible Ecad. Nevertheless, the existence of other sites of intestinal translocation as well as the precise molecular mechanism by which *Lm* is actually transferred across the intestinal barrier monolayer have so far not been addressed. This prompted us to set up an experimental approach based on the comprehensive imaging of uninfected and infected intestinal tissues of *iFABP*-hEcad transgenic mice. This approach preserves the intrinsic cell heterogeneity in a tissue context, allowing us to perform a detailed study of the initial steps of *Lm* invasion and of the mechanisms of translocation across the intestinal epithelium with a level of scrutiny usually reserved for cultured cells. We demonstrate that Ecad is luminally accessible at cell–cell junctions between mucus-expelling GCs and adjacent enterocytes all along the vertical axis of intestinal villi. We show that *Lm* accesses the intestinal lamina propria mostly all along the villus longitudinal axis and mainly targets luminally accessible Ecad of GCs to adhere to and invade the intestinal epithelium in an InlA-dependent manner. We demonstrate that *Lm* is then rapidly translocated from the apical to basolateral side of IECs enclosed in a vacuole. This translocation is microtubule dependent but independent of the virulence factors LLO and ActA. Furthermore, the exocytic machinery is involved in *Lm* release in the lamina propria. Finally, *Lm* rapid transepithelial transcytosis leads to a similarly rapid systemic dissemination. Together, these results demonstrate that *Lm* is transcytosed across the intestinal epithelium (Fig. S6 B), thus revealing a novel and unsuspected pathway hijacked by *Lm* that is crucial for its rapid dissemination within the host.

We have identified novel in vivo sites of accessible Ecad around GCs, at cell–cell junctions with their neighbors, and along villus epithelial folds. Moreover, as previously reported in vitro (Pentecost et al., 2006, 2010), we found that Ecad is luminally accessible at cell extrusion sites. In a similar fashion as extruding cells, mucus-producing GCs undergo extensive shape changes such as stretch and compression during mucus secretion. These shape changes are accompanied with junctional reorganization, notably variations in length and strand cross-linking and discontinuities (Hull and Staehelin, 1976; Madara and Trier, 1982; Porvaznik et al., 1983; Madara, 1990). Accordingly, we demonstrate here that TJs are disorganized between cells on which Ecad is luminally exposed and establish a correlation between mucus secretion and luminal access to Ecad. Furthermore, cortical actin at the apex of GCs is greatly reduced compared with IECs (Oliver and Specian, 1990). We indeed observed a reorganized apical actin network at sites with accessible Ecad (Fig. S4 M), a result which is consistent with the well-established importance of the actin cytoskeleton in maintaining cell junction integrity by stabilizing Ecad clusters (Hagen and Trier, 1988; Cavey et al., 2008; Schill and Anderson, 2009). Finally, we also show that Ecad is luminally accessible in villus intestinal folds (Fig. S4 I and Video 9). The forces of tension and constriction generated at these sites induce cell shape changes that may account for the relocation of Ecad to the apical luminal side, as previously described for adherens junction protein remodeling occurring during *Drosophila* gastrulation and ventral furrow formation (Dawes-Hoang et al., 2005; Kölsch et al., 2007). Altogether, our investigations point to a correlation between physical tensions, localization of adherens junction components and TJ remodeling at the intestinal epithelium level. *Lm* targeting of accessible Ecad illustrates how a microbial pathogen can take advantage of tissue dynamics and heterogeneity in vivo, a facet of microbial pathogenesis which cannot be investigated in vitro in more static and homogenous systems.

We have demonstrated *Lm* preferential targeting of GC accessible Ecad and a correlation between GC numbers and *Lm* intestinal invasion and systemic dissemination. Even though mucus secretion is at the front line of the innate host defense in the gastrointestinal tract, *Lm* seems to exploit this innate defense mechanism by binding in an InlA-dependent manner to GCs. Moreover, although GCs are specialized in basal-apical transport, they also possess an endocytic and apicobasal transcytosis activity that *Lm* may hijack (Colony and Specian, 1987). Thus, *Lm* takes advantage of an intestinal

defense mechanism, namely mucus secretion, to target and cross the epithelium by transcytosis, uncovering an unsuspected Achilles' heel of the innate immune system that *Lm* has evolved to take advantage of. Nevertheless, we have also observed that *Lm* interacts with intestinal GCs not expressing accessible Ecad, although this is far less frequent than with GCs that express accessible Ecad (Fig. 4 C). It has been previously reported that other internalins of *Lm*, such as InlB, InlC, and InlJ, contain mucin-binding domains able to bind secreted Mucin-2 (Lindén et al., 2008). However, they do not bind to the membrane-bound Mucin-1, suggesting that *Lm* attraction to GCs in vivo is not caused by Inl–Muc interactions, but rather results from InlA–Ecad interactions. However, Inl–Muc interactions may retain *Lm* within the mucus layer in an environment close to their source, the GCs, thus facilitating InlA–Ecad-mediated bacterial adhesion. This is further supported by the >15-fold increase of relative infection of accessible Ecad-expressing GCs compared with Δ*inlA* interactions with GCs (Fig. 4 C).

In vitro studies have shown that bacteria can transcytose across cultured cell monolayers, including *Campylobacter jejuni* (Grant et al., 1993; Russell and Blake, 1994; Bacon et al., 2001; Kopecko et al., 2001; Hu et al., 2008; Watson and Galán, 2008), *Neisseria gonorrhoeae* and *Neisseria meningitidis* (Makino et al., 1991; Merz and So, 2000; Kuespert et al., 2006; Wang et al., 2008; Sutherland et al., 2010), *Streptococcus pneumoniae* (Zhang et al., 2000; Kaetzel, 2001), and *Escherichia coli* (Burns et al., 2001; Xie et al., 2004). Yet, with the exception of bacterial sampling by M cells (see next paragraph), this is the first time to our knowledge that a bacterium has been shown to translocate across an epithelial layer by transcytosis in vivo, resulting in its systemic dissemination. That *Lm* follows a transcytosis pathway rather than its classical infection cycle was unexpected, as *Lm* is considered a prototypic intracytosolic pathogen (Fig. S6 A). Yet, having evolved such a furtive means to cross the intestinal barrier seems perfectly in line with the observed rapidity of *Lm* transepithelial transfer, the absence of intraepithelial bacterial proliferation and epithelial damage during the intestinal phase of listeriosis, and the fact that actin-based motility directionality does not preferentially route *Lm* to the basal pole of enterocytes. But why doesn't *Lm* escape its vacuole at the intestinal epithelium level to cross the intestinal epithelium? It could be that transcytosis is too rapid to allow LLO-dependent *Lm* escape from its internalization vacuole. In addition, it has been recently shown in macrophages that LLO activity is activated by GILT (Singh et al., 2008). GILT is constitutively expressed in antigen-presenting cells and is inducible by IFN-γ in other cell types (Arunachalam et al., 2000). Because GILT is not constitutively expressed in enterocytes, it may not activate LLO early on in the infection, thus allowing the *Lm*-containing vacuole to be transcytosed apicobasally. Later on, as IFN-γ expression is triggered, GILT induction would lead to the activation of LLO, allowing *Lm* to be diverted from transcytosis and delivered into the cytosol. In line with this hypothesis, intracytosolic *Lm* can be observed in vivo in enterocytes later on in the infection (Lecuit et al., 2001; Pentecost et al., 2006, 2010).

We also show here that inhibition of NSF blocks the release of *Lm* in the lamina propria and consequently its exit from epithelial cells. NSF and soluble NSF attachment proteins (SNAPs) are essential components of the intracellular membrane fusion apparatus (Jahn and Scheller, 2006). This suggests that *Lm*-containing vacuoles fuse with the basolateral membrane and exocytose, releasing *Lm* subepithelially. There are only two in vitro studies illustrating bacterial exocytosis, by means of electron microscopy pictures of *C. jejuni* (Hu et al., 2008; Baker and Graham, 2010), but the putative role of the exocytic machinery in bacterial escape has not been addressed in vivo in the context of a bacterial infection. *Lm* seems to exploit the full range of Ecad recycling, not only by mimicking its natural ligand Ecad, binding to it and inducing its internalization, but also by subverting its basolateral recycling in polarized epithelial cells by transcytosis and exocytosis.

Lm transcytosis is strictly InlA dependent and LLO independent, whereas we have shown that the intestinal host response to *Lm* is InlA independent and strictly LLO dependent (Lecuit et al., 2007). We can interpret these findings as follows: at the intestinal villus level, in which *Lm* enters via InlA without inducing tissue damage, the bacterium follows a furtive intravacuolar path that avoids detection by cytosolic sensors and remains undetected in the lamina propria, possibly because of its extracellular location and its ability to escape innate immune system recognition (Boneca et al., 2007; Gouin et al., 2010; Personnic et al., 2010). In contrast, after translocation through M cells in an InlA-independent manner (Pron et al., 1998; Lecuit et al., 2001; Corr et al., 2006; Chiba et al., 2011), *Lm* is phagocytosed by antigen-presenting cells, where LLO mediates vacuolar rupture, switching on the host response. This scenario illustrates how *Lm* has evolved mechanisms that allow its dissemination into the host via the intestinal lamina propria without inducing, at least initially, strong innate immune responses. This is in sharp contrast with enteropathogens such as *Shigella flexneri* that are contained at the intestinal level to the expense of strong and destructive inflammation responses.

Lm is a model microorganism that has been particularly instrumental for key discoveries in the fields of microbiology, cell biology, and immunology. By extending the cellular microbiology approach to tissues and by using high-resolution tissue-imaging techniques, we have demonstrated that the well-established dogma of *Lm* access to the cytosol for host tissue invasion does not apply to its early, rapid, and efficient crossing of the intestinal barrier. These results not only revisit and enrich our understanding of *Lm* pathogenesis, but also provide new clues as to how microbial pathogens breach host barriers. Future investigations will have to focus on the mechanisms of *Lm* breaching of the placental and blood-brain barriers and also on how other microbial pathogens cross host barriers.

MATERIALS AND METHODS

Bacterial strains and culture conditions. Bacterial strains used in this study are *Lm* strain EGD (BUG 600), its isogenic deletion mutants Δ*inlA* (BUG 947), Δ*hly* (BUG 1954), and Δ*actA* (BUG 2140), and *Li* WT (BUG 499) and *Li*-expressing InlA (BUG 1489). The inocula used are shown in figure legends and are 1–3 × 10^9 per intestinal ligated loop. Bacteria were cultured as described previously (Disson et al., 2009).

Animals. We used transgenic mice expressing hEcad on a C57BL/6 genetic background (Lecuit et al., 2001). To generate mice expressing both a membrane-targeted Tomato protein and the humanized E16P Ecad, mT/mG mice were crossed with E16P KI mice (Charles River; Muzumdar et al., 2007; Disson et al., 2008). Animal experiments were performed according to the Institut Pasteur guidelines for laboratory animals' husbandry. For intestinal ligated loops, 8–12-wk-old mice were fasted for 16 h before surgery. After mild anesthesia of mice with 2.5% (vol/vol) vaporous isoflurane (Aerrane; Baxter), deep anesthesia was induced with a mix of ketamine (50 mg/kg body weight; Imalgene 1000; Merial) and medetomidine (0.5 mg/kg body weight; Domitor; Orion Corporation). A laparotomy was performed, the small intestine was exposed, and jejunal loops of 3 cm long were prepared. 200 µl of inoculum was injected into each loop. At the planned endpoint, the animal was euthanized, and intestinal loops were harvested, opened longitudinally, washed repeatedly in 37°C Dulbecco's modified Eagle's medium (Invitrogen), and fixed flat (luminal side up) in 35 × 10–mm tissue culture dishes (BD) containing 4% agarose (Sigma-Aldrich). For IL-33 administration, 400 ng of recombinant mouse IL-33 (R&D Systems) in PBS were administered daily for 3 d intraperitoneally. Intestinal ligated loops were performed 24 h later after the last injection. Control animals received PBS only.

All the procedures were in agreement with the guidelines of the European Commission for the handling of laboratory animals, directive 86/609/EEC (http://ec.europa.eu/environment/chemicals/lab_animals/home_en.htm) and were approved by the Animal Care and Use Committee of the Institut Pasteur.

Enumeration of CFUs. For CFU enumeration, the organs were retrieved and grounded, and serial dilutions were plated on BHI (brain heart infusion) agar plates as previously described (Disson et al., 2009).

Pharmacological treatments. For microtubule depolymerization and inhibition of polymerization, 10 µg/ml nocodazole and 10 µg/ml colchicine (Sigma-Aldrich) were used per ligated loop (Mostov et al., 1984; Ameen et al., 2003; Wang et al., 2008). Loops were initially infected for 10 min and, subsequently, nocodazole or colchicine was added and kept along the infection (50 min). For exocytosis inhibition, we used 20 µg/ml of the recombinant NSF peptide TAT-NSF_{700} (AnaSpec). This peptide has been described to be the most potent peptide to enter cells and inhibit NSF-mediated ATPase activity and SNARE complex disassembly.TAT-NSF_{700}scr (AnaSpec) is a control peptide that does not inhibit NSF activity (Matsushita et al., 2003, 2005). The TAT-NSF_{700} peptide conjugated to cyanin 3 (R.D-Biotech) was used to verify the entry of the peptide in cells.

Tissue labeling for immunofluorescence. Tissues were fixed in 4% paraformaldehyde (Electron Microscopy Sciences) in PBS for 1 h at room temperature under agitation and either stained directly (whole mount) or embedded in 4% low-melting-point agarose (Sigma-Aldrich) for 100–250-µm-thick vibratome sections (Micro HM 650V; Thermo Fisher Scientific; Appleton et al., 2009). Sections were stained in a similar manner to whole mount tissue but mounted in fluorescent mounting medium (Fluoromount; Interchim). Tissues were permeabilized for 1 h in 0.4% Triton X-100 (Sigma-Aldrich) and 3% PBS-BSA (Sigma-Aldrich) or preincubated for 1 h in the blocking buffer 3% PBS-BSA. Then tissues were labeled with the appropriate primary and secondary antibody overnight at 4°C and 2 h at room temperature, respectively.

To label accessible Ecad of uninfected tissues, tissues were directly recovered without intestinal ligation to avoid ischemic and epithelial damages, fixed in 4% paraformaldehyde as described in the previous paragraph, and labeled. To detect accessible hEcad, we used HECD-1, a specific mouse mAb raised against the extracellular domain of hEcad (Invitrogen). To detect accessible mEcad, we used ECCD-2, a specific rat mAb raised against the extracellular domain of mEcad (Invitrogen). We used an antibody against the cytoplasmic domain of Ecad (36/Ecad mouse mAb; BD) to show the association of *Lm* with a membrane vacuole because internalized Ecad decorates the vacuolar membrane.

For Sytox staining, 1 µM Sytox green (Invitrogen) was injected into an intestinal ligated loop for 30 min. The tissue was then harvested, fixed, and processed as described above for further staining.

For immunofluorescence of cryosections, retrieved tissues were fixed and embedded in OCT compound at −80°C (Tissue-Tek), cut using a cryostat at −20°C (7-µm-thick sections), postfixed in pure ethanol, and labeled with the appropriate primary and secondary antibody for 1 h at room temperature and 2 h at room temperature, respectively. Sections were mounted in fluorescent mounting medium (Fluoromount).

Microscopy. Samples were imaged with an upright LSM510 two-photon META (Carl Zeiss) or with an LSM700 confocal microscope (Carl Zeiss) with a 40× water immersion objective. Image analysis was performed using ImageJ (National Institutes of Health), LSM 5 Image Browser (Carl Zeiss), and Photoshop software (Adobe). Three-dimensional reconstructions were performed using Imaris 5.5.3 software (Bitplane).

TEM. Infected intestinal tissues were washed in PBS and fixed in 2.5% glutaraldehyde–0.1 M cacodylate buffer solution overnight at 4°C. Fixed tissues were washed three times in cacodylate buffer and then fixed for 1 h at room temperature in 1% OsO_4 in the same buffer. Fixed tissues were washed once in cacodylate buffer and twice in distilled water. After dehydration in an ethanol-graded series and in propylene oxide, tissues were embedded in epoxy resin. Specimens were cut using an ultramicrotome Reichert Ultracut S. 60-nm sections were picked up on Formvar regular mesh grids, contrasted with uranyl acetate and lead citrate, and observed on a JEM 1010 (JEOL) under standard conditions at 60 kV.

Calculation of *Lm* associations with cell subtypes. Ligated loops were fixed 40 min p.i. and labeled with WGA and for accessible hEcad and *Lm*. The relative proportions of GCs, NGCs, and AGCs were calculated (see Results). The amount of *Lm* per cell for each cell subtype was determined, taking into account the accessibility of hEcad. We finally calculated the number of *Lm* per cell type relative to the respective abundance of each cell type and normalized to *Lm* associations with AGCs (Fig. 4 C).

Antibodies and fluorescent probes. The following pAbs, mAbs, and other fluorescent probes were used for immunolabeling of tissues: anti–hEcad clone HECD-1 mouse mAb (Invitrogen), anti-Ecad clone 36/Ecad mouse mAb (BD), anti–mEcad clone ECCD-2 rat mAb (Invitrogen), anti–ZO-1 rabbit pAb (Invitrogen), anti-occludin rabbit pAb (Invitrogen), anti-PARD3A (H-70) rabbit pAb (Santa Cruz Biotechnology, Inc.), anti–PKCζ (C-20) rabbit pAb (Santa Cruz Biotechnology, Inc.), anti-ITF (M-18) goat pAb (Santa Cruz Biotechnology, Inc.), anti–Mucin 2 (R-12) goat pAb (Santa Cruz Biotechnology, Inc.), WGA conjugated with Alexa Fluor 555, Alexa Fluor 647, or Alexa Fluor 488 (Invitrogen), Alexa Fluor 647 or Alexa Fluor 488 phalloidin (Invitrogen), Hoechst 33342 (Invitrogen), Alexa Fluor 488 or Alexa Fluor 546 goat anti–rabbit, Alexa Fluor 488 or Alexa Fluor 546 goat anti–mouse, Alexa Fluor 488 goat anti–rat, donkey anti–goat-FITC, donkey anti–goat-rhodamine, and TUNEL (in situ cell death detection kit fluorescein; Roche).

Statistics. Values are expressed as mean ± SD. Statistical comparisons were made using two-way analysis of variance with Tukey adjustment for multiple comparisons and timed data analysis (Olsen, 2003) or using a Student's *t* test for single comparisons.

Online supplemental material. Fig. S1 shows that Ecad accessibility is an intrinsic property of intestinal villus epithelium. Fig. S2 shows that WGA^{hi} cells are GCs, lack apical actin cytoskeleton, and are stained for

GC-specific markers ITF and Muc-2. Fig. S3 shows additional pictures of GC disorganized TJs. Fig. S4 shows the characterization of non-GC subpopulations expressing luminally accessible Ecad. Fig. S5 shows that nocodazole treatment does not affect adherens junction and TJ integrity. Fig. S6 represents the *Lm* cell infectious process in vitro and in vivo. Videos 1 and 2 show three-dimensional reconstructions of a noninfected and an *Lm*-infected intestinal villus. Videos 3 and 4 show accessible Ecad on an intestinal villus and on a GC. Videos 5–7 show TJ disorganization on GCs. Videos 8 and 9 show accessible Ecad on non-GC subpopulations. Table S1 summarizes TJ characteristics around cells expressing luminally accessible Ecad. Online supplemental material is available at http://www.jem.org/cgi/content/full/jem.20110560/DC1.

We thank the members of the Microbes and Host Barriers Group for their support and Matteo Bonazzi and the personnel of the Imagopole Facility for their help and support. We thank Gerard Eberl for helpful discussion and advice.

Georgios Nikitas received a Marie Curie Early Stage Research Training fellowship from the Intrapath program, EU FP6. We thank Institut Pasteur, Institut National de la Santé et de la Recherche Médicale, Fondation pour la Recherche Médicale, Ville de Paris, Fondation BNP Paribas, and the European Research Council for financial support.

The authors declare that they have no competing financial interests.

Submitted: 21 March 2011
Accepted: 1 September 2011

REFERENCES

Ameen, N.A., C. Marino, and P.J. Salas. 2003. cAMP-dependent exocytosis and vesicle traffic regulate CFTR and fluid transport in rat jejunum in vivo. *Am. J. Physiol. Cell Physiol.* 284:C429–C438.

Appleton, P.L., A.J. Quyn, S. Swift, and I. Näthke. 2009. Preparation of wholemount mouse intestine for high-resolution three-dimensional imaging using two-photon microscopy. *J. Microsc.* 234:196–204. http://dx.doi.org/10.1111/j.1365-2818.2009.03163.x

Arunachalam, B., U.T. Phan, H.J. Geuze, and P. Cresswell. 2000. Enzymatic reduction of disulfide bonds in lysosomes: characterization of a gamma-interferon-inducible lysosomal thiol reductase (GILT). *Proc. Natl. Acad. Sci. USA.* 97:745–750. http://dx.doi.org/10.1073/pnas.97.2.745

Bacon, D.J., C.M. Szymanski, D.H. Burr, R.P. Silver, R.A. Alm, and P. Guerry. 2001. A phase-variable capsule is involved in virulence of *Campylobacter jejuni* 81-176. *Mol. Microbiol.* 40:769–777. http://dx.doi.org/10.1046/j.1365-2958.2001.02431.x

Baker, N.T., and L.L. Graham. 2010. *Campylobacter* fetus translocation across Caco-2 cell monolayers. *Microb. Pathog.* 49:260–272. http://dx.doi.org/10.1016/j.micpath.2010.06.008

Boller, K., D. Vestweber, and R. Kemler. 1985. Cell-adhesion molecule uvomorulin is localized in the intermediate junctions of adult intestinal epithelial cells. *J. Cell Biol.* 100:327–332. http://dx.doi.org/10.1083/jcb.100.1.327

Boneca, I.G., O. Dussurget, D. Cabanes, M.A. Nahori, S. Sousa, M. Lecuit, E. Psylinakis, V. Bouriotis, J.P. Hugot, M. Giovannini, et al. 2007. A critical role for peptidoglycan N-deacetylation in *Listeria* evasion from the host innate immune system. *Proc. Natl. Acad. Sci. USA.* 104:997–1002. http://dx.doi.org/10.1073/pnas.0609672104

Burns, J.L., A. Griffith, J.J. Barry, M. Jonas, and E.Y. Chi. 2001. Transcytosis of gastrointestinal epithelial cells by *Escherichia coli* K1. *Pediatr. Res.* 49:30–37. http://dx.doi.org/10.1203/00006450-200101000-00010

Cavey, M., M. Rauzi, P.F. Lenne, and T. Lecuit. 2008. A two-tiered mechanism for stabilization and immobilization of E-cadherin. *Nature.* 453:751–756. http://dx.doi.org/10.1038/nature06953

Chiba, S., T. Nagai, T. Hayashi, Y. Baba, S. Nagai, and S. Koyasu. 2011. Listerial invasion protein internalin B promotes entry into ileal Peyer's patches in vivo. *Microbiol. Immunol.* 55:123–129. http://dx.doi.org/10.1111/j.1348-0421.2010.00292.x

Colony, P.C., and R.D. Specian. 1987. Endocytosis and vesicular traffic in fetal and adult colonic goblet cells. *Anat. Rec.* 218:365–372. http://dx.doi.org/10.1002/ar.1092180403

Corr, S., C. Hill, and C.G. Gahan. 2006. An in vitro cell-culture model demonstrates internalin- and hemolysin-independent translocation of *Listeria monocytogenes* across M cells. *Microb. Pathog.* 41:241–250. http://dx.doi.org/10.1016/j.micpath.2006.08.003

Cossart, P., and P.J. Sansonetti. 2004. Bacterial invasion: the paradigms of enteroinvasive pathogens. *Science.* 304:242–248. http://dx.doi.org/10.1126/science.1090124

Dawes-Hoang, R.E., K.M. Parmar, A.E. Christiansen, C.B. Phelps, A.H. Brand, and E.F. Wieschaus. 2005. Folded gastrulation, cell shape change and the control of myosin localization. *Development.* 132:4165–4178. http://dx.doi.org/10.1242/dev.01938

De Brabander, M.J., R.M. Van de Veire, F.E. Aerts, M. Borgers, and P.A. Janssen. 1976. The effects of methyl (5-(2-thienylcarbonyl)-1H-benzimidazol-2-yl) carbamate, (R 17934; NSC 238159), a new synthetic antitumoral drug interfering with microtubules, on mammalian cells cultured in vitro. *Cancer Res.* 36:905–916.

Disson, O., S. Grayo, E. Huillet, G. Nikitas, F. Langa-Vives, O. Dussurget, M. Ragon, A. Le Monnier, C. Babinet, P. Cossart, and M. Lecuit. 2008. Conjugated action of two species-specific invasion proteins for fetoplacental listeriosis. *Nature.* 455:1114–1118. http://dx.doi.org/10.1038/nature07303

Disson, O., G. Nikitas, S. Grayo, O. Dussurget, P. Cossart, and M. Lecuit. 2009. Modeling human listeriosis in natural and genetically engineered animals. *Nat. Protoc.* 4:799–810. http://dx.doi.org/10.1038/nprot.2009.66

Fischer, J., P.J. Klein, M. Vierbuchen, B. Skutta, G. Uhlenbruck, and R. Fischer. 1984. Characterization of glycoconjugates of human gastrointestinal mucosa by lectins. I. Histochemical distribution of lectin binding sites in normal alimentary tract as well as in benign and malignant gastric neoplasms. *J. Histochem. Cytochem.* 32:681–689. http://dx.doi.org/10.1177/32.7.6330198

Garcia-del Portillo, F., and B.B. Finlay. 1995. Targeting of *Salmonella typhimurium* to vesicles containing lysosomal membrane glycoproteins bypasses compartments with mannose 6-phosphate receptors. *J. Cell Biol.* 129:81–97. http://dx.doi.org/10.1083/jcb.129.1.81

Gouin, E., M. Adib-Conquy, D. Balestrino, M.A. Nahori, V. Villiers, F. Colland, S. Dramsi, O. Dussurget, and P. Cossart. 2010. The *Listeria monocytogenes* InlC protein interferes with innate immune responses by targeting the IkappaB kinase subunit IKKalpha. *Proc. Natl. Acad. Sci. USA.* 107:17333–17338. http://dx.doi.org/10.1073/pnas.1007765107

Grant, C.C., M.E. Konkel, W. Cieplak Jr., and L.S. Tompkins. 1993. Role of flagella in adherence, internalization, and translocation of *Campylobacter jejuni* in nonpolarized and polarized epithelial cell cultures. *Infect. Immun.* 61:1764–1771.

Hagen, S.J., and J.S. Trier. 1988. Immunocytochemical localization of actin in epithelial cells of rat small intestine by light and electron microscopy. *J. Histochem. Cytochem.* 36:717–727. http://dx.doi.org/10.1177/36.7.3290330

Henry, R., L. Shaughnessy, M.J. Loessner, C. Alberti-Segui, D.E. Higgins, and J.A. Swanson. 2006. Cytolysin-dependent delay of vacuole maturation in macrophages infected with *Listeria monocytogenes*. *Cell. Microbiol.* 8:107–119. http://dx.doi.org/10.1111/j.1462-5822.2005.00604.x

Hirose, T., Y. Izumi, Y. Nagashima, Y. Tamai-Nagai, H. Kurihara, T. Sakai, Y. Suzuki, T. Yamanaka, A. Suzuki, K. Mizuno, and S. Ohno. 2002. Involvement of ASIP/PAR-3 in the promotion of epithelial tight junction formation. *J. Cell Sci.* 115:2485–2495.

Hu, L., B.D. Tall, S.K. Curtis, and D.J. Kopecko. 2008. Enhanced microscopic definition of *Campylobacter jejuni* 81-176 adherence to, invasion of, translocation across, and exocytosis from polarized human intestinal Caco-2 cells. *Infect. Immun.* 76:5294–5304. http://dx.doi.org/10.1128/IAI.01408-07

Hull, B.E., and L.A. Staehelin. 1976. Functional significance of the variations in the geometrical organization of tight junction networks. *J. Cell Biol.* 68:688–704. http://dx.doi.org/10.1083/jcb.68.3.688

Izumi, Y., T. Hirose, Y. Tamai, S. Hirai, Y. Nagashima, T. Fujimoto, Y. Tabuse, K.J. Kemphues, and S. Ohno. 1998. An atypical PKC directly associates and colocalizes at the epithelial tight junction with ASIP, a mammalian homologue of *Caenorhabditis elegans* polarity protein PAR-3. *J. Cell Biol.* 143:95–106. http://dx.doi.org/10.1083/jcb.143.1.95

Jahn, R., and R.H. Scheller. 2006. SNAREs—engines for membrane fusion. *Nat. Rev. Mol. Cell Biol.* 7:631–643. http://dx.doi.org/10.1038/nrm2002

Jang, M.H., M.N. Kweon, K. Iwatani, M. Yamamoto, K. Terahara, C. Sasakawa, T. Suzuki, T. Nochi, Y. Yokota, P.D. Rennert, et al. 2004. Intestinal villous M cells: an antigen entry site in the mucosal epithelium. *Proc. Natl. Acad. Sci. USA*. 101:6110–6115. http://dx.doi.org/10.1073/pnas.0400969101

Kaetzel, C.S. 2001. Polymeric Ig receptor: defender of the fort or Trojan horse? *Curr. Biol.* 11:R35–R38. http://dx.doi.org/10.1016/S0960-9822(00)00041-5

Kocks, C., E. Gouin, M. Tabouret, P. Berche, H. Ohayon, and P. Cossart. 1992. *L. monocytogenes*-induced actin assembly requires the actA gene product, a surface protein. *Cell*. 68:521–531. http://dx.doi.org/10.1016/0092-8674(92)90188-I

Kölsch, V., T. Seher, G.J. Fernandez-Ballester, L. Serrano, and M. Leptin. 2007. Control of *Drosophila* gastrulation by apical localization of adherens junctions and RhoGEF2. *Science*. 315:384–386. http://dx.doi.org/10.1126/science.1134833

Kopecko, D.J., L. Hu, and K.J. Zaal. 2001. *Campylobacter jejuni*—microtubule-dependent invasion. *Trends Microbiol.* 9:389–396. http://dx.doi.org/10.1016/S0966-842X(01)02107-2

Kuespert, K., S. Pils, and C.R. Hauck. 2006. CEACAMs: their role in physiology and pathophysiology. *Curr. Opin. Cell Biol.* 18:565–571. http://dx.doi.org/10.1016/j.ceb.2006.08.008

Lecuit, M., S. Dramsi, C. Gottardi, M. Fedor-Chaiken, B. Gumbiner, and P. Cossart. 1999. A single amino acid in E-cadherin responsible for host specificity towards the human pathogen *Listeria monocytogenes*. *EMBO J.* 18:3956–3963. http://dx.doi.org/10.1093/emboj/18.14.3956

Lecuit, M., S. Vandormael-Pournin, J. Lefort, M. Huerre, P. Gounon, C. Dupuy, C. Babinet, and P. Cossart. 2001. A transgenic model for listeriosis: role of internalin in crossing the intestinal barrier. *Science*. 292:1722–1725. http://dx.doi.org/10.1126/science.1059852

Lecuit, M., J.L. Sonnenburg, P. Cossart, and J.I. Gordon. 2007. Functional genomic studies of the intestinal response to a foodborne enteropathogen in a humanized gnotobiotic mouse model. *J. Biol. Chem.* 282:15065–15072. http://dx.doi.org/10.1074/jbc.M610926200

Lee, J.C., D.J. Field, and L.L. Lee. 1980. Effects of nocodazole on structures of calf brain tubulin. *Biochemistry*. 19:6209–6215. http://dx.doi.org/10.1021/bi00567a041

Lindén, S.K., H. Bierne, C. Sabet, C.W. Png, T.H. Florin, M.A. McGuckin, and P. Cossart. 2008. *Listeria monocytogenes* internalins bind to the human intestinal mucin MUC2. *Arch. Microbiol.* 190:101–104. http://dx.doi.org/10.1007/s00203-008-0358-6

Madara, J.L. 1990. Maintenance of the macromolecular barrier at cell extrusion sites in intestinal epithelium: physiological rearrangement of tight junctions. *J. Membr. Biol.* 116:177–184. http://dx.doi.org/10.1007/BF01868675

Madara, J.L., and J.S. Trier. 1982. Structure and permeability of goblet cell tight junctions in rat small intestine. *J. Membr. Biol.* 66:145–157. http://dx.doi.org/10.1007/BF01868490

Madara, J.L., J.S. Trier, and M.R. Neutra. 1980. Structural changes in the plasma membrane accompanying differentiation of epithelial cells in human and monkey small intestine. *Gastroenterology*. 78:963–975.

Makino, S., J.P. van Putten, and T.F. Meyer. 1991. Phase variation of the opacity outer membrane protein controls invasion by *Neisseria gonorrhoeae* into human epithelial cells. *EMBO J.* 10:1307–1315.

Marchiando, A.M., L. Shen, W.V. Graham, K.L. Edelblum, C.A. Duckworth, Y. Guan, M.H. Montrose, J.R. Turner, and A.J. Watson. 2011. The epithelial barrier is maintained by in vivo tight junction expansion during pathologic intestinal epithelial shedding. *Gastroenterology*. 140:1208–1218. http://dx.doi.org/10.1053/j.gastro.2011.01.004

Matsushita, K., C.N. Morrell, B. Cambien, S.X. Yang, M. Yamakuchi, C. Bao, M.R. Hara, R.A. Quick, W. Cao, B. O'Rourke, et al. 2003. Nitric oxide regulates exocytosis by S-nitrosylation of N-ethylmaleimide-sensitive factor. *Cell*. 115:139–150. http://dx.doi.org/10.1016/S0092-8674(03)00803-1

Matsushita, K., C.N. Morrell, and C.J. Lowenstein. 2005. A novel class of fusion polypeptides inhibits exocytosis. *Mol. Pharmacol.* 67:1137–1144. http://dx.doi.org/10.1124/mol.104.004275

Mengaud, J., H. Ohayon, P. Gounon, R.-M. Mege, and P. Cossart. 1996. E-cadherin is the receptor for internalin, a surface protein required for entry of *L. monocytogenes* into epithelial cells. *Cell*. 84:923–932. http://dx.doi.org/10.1016/S0092-8674(00)81070-3

Merz, A.J., and M. So. 2000. Interactions of pathogenic *Neisseriae* with epithelial cell membranes. *Annu. Rev. Cell Dev. Biol.* 16:423–457. http://dx.doi.org/10.1146/annurev.cellbio.16.1.423

Moro, K., T. Yamada, M. Tanabe, T. Takeuchi, T. Ikawa, H. Kawamoto, J. Furusawa, M. Ohtani, H. Fujii, and S. Koyasu. 2010. Innate production of T(H)2 cytokines by adipose tissue-associated c-Kit(+)Sca-1(+) lymphoid cells. *Nature*. 463:540–544. http://dx.doi.org/10.1038/nature08636

Mostov, K.E., M. Friedlander, and G. Blobel. 1984. The receptor for transepithelial transport of IgA and IgM contains multiple immunoglobulin-like domains. *Nature*. 308:37–43. http://dx.doi.org/10.1038/308037a0

Muzumdar, M.D., B. Tasic, K. Miyamichi, L. Li, and L. Luo. 2007. A global double-fluorescent Cre reporter mouse. *Genesis*. 45:593–605. http://dx.doi.org/10.1002/dvg.20335

Myers, J.T., A.W. Tsang, and J.A. Swanson. 2003. Localized reactive oxygen and nitrogen intermediates inhibit escape of *Listeria monocytogenes* from vacuoles in activated macrophages. *J. Immunol.* 171:5447–5453.

Neill, D.R., S.H. Wong, A. Bellosi, R.J. Flynn, M. Daly, T.K. Langford, C. Bucks, C.M. Kane, P.G. Fallon, R. Pannell, et al. 2010. Nuocytes represent a new innate effector leukocyte that mediates type-2 immunity. *Nature*. 464:1367–1370. http://dx.doi.org/10.1038/nature08900

Ohno, S. 2001. Intercellular junctions and cellular polarity: the PAR-aPKC complex, a conserved core cassette playing fundamental roles in cell polarity. *Curr. Opin. Cell Biol.* 13:641–648. http://dx.doi.org/10.1016/S0955-0674(00)00264-7

Oliver, M.G., and R.D. Specian. 1990. Cytoskeleton of intestinal goblet cells: role of actin filaments in baseline secretion. *Am. J. Physiol.* 259:G991–G997.

Olsen, C.H. 2003. Review of the use of statistics in infection and immunity. *Infect. Immun.* 71:6689–6692. http://dx.doi.org/10.1128/IAI.71.12.6689-6692.2003

Pentecost, M., G. Otto, J.A. Theriot, and M.R. Amieva. 2006. *Listeria monocytogenes* invades the epithelial junctions at sites of cell extrusion. *PLoS Pathog.* 2:e3. http://dx.doi.org/10.1371/journal.ppat.0020003

Pentecost, M., J. Kumaran, P. Ghosh, and M.R. Amieva. 2010. *Listeria monocytogenes* internalin B activates junctional endocytosis to accelerate intestinal invasion. *PLoS Pathog.* 6:e1000900. http://dx.doi.org/10.1371/journal.ppat.1000900

Personnic, N., S. Bruck, M.A. Nahori, A. Toledo-Arana, G. Nikitas, M. Lecuit, O. Dussurget, P. Cossart, and H. Bierne. 2010. The stress-induced virulence protein InlH controls interleukin-6 production during murine listeriosis. *Infect. Immun.* 78:1979–1989. http://dx.doi.org/10.1128/IAI.01096-09

Porvaznik, M., W. Baker, and R.I. Walker. 1983. Disruption of the goblet cell intercellular junction following histamine infusion of the rabbit ileum. *Experientia*. 39:514–518. http://dx.doi.org/10.1007/BF01965183

Poulsom, R., and N.A. Wright. 1993. Trefoil peptides: a newly recognized family of epithelial mucin-associated molecules. *Am. J. Physiol.* 265:G205–G213.

Pron, B., C. Boumaila, F. Jaubert, S. Sarnacki, J.P. Monnet, P. Berche, and J.L. Gaillard. 1998. Comprehensive study of the intestinal stage of listeriosis in a rat ligated ileal loop system. *Infect. Immun.* 66:747–755.

Ravelli, R.B., B. Gigant, P.A. Curmi, I. Jourdain, S. Lachkar, A. Sobel, and M. Knossow. 2004. Insight into tubulin regulation from a complex with colchicine and a stathmin-like domain. *Nature*. 428:198–202. http://dx.doi.org/10.1038/nature02393

Russell, R.G., and D.C. Blake Jr. 1994. Cell association and invasion of Caco-2 cells by *Campylobacter jejuni*. *Infect. Immun.* 62:3773–3779.

Schiff, P.B., and S.B. Horwitz. 1980. Taxol stabilizes microtubules in mouse fibroblast cells. *Proc. Natl. Acad. Sci. USA*. 77:1561–1565. http://dx.doi.org/10.1073/pnas.77.3.1561

Schill, N.J., and R.A. Anderson. 2009. Out, in and back again: PtdIns(4,5)P(2) regulates cadherin trafficking in epithelial morphogenesis. *Biochem. J.* 418:247–260. http://dx.doi.org/10.1042/BJ20081844

Singh, R., A. Jamieson, and P. Cresswell. 2008. GILT is a critical host factor for *Listeria monocytogenes* infection. *Nature*. 455:1244–1247. http://dx.doi.org/10.1038/nature07344

Sousa, S., M. Lecuit, and P. Cossart. 2005. Microbial strategies to target, cross or disrupt epithelia. *Curr. Opin. Cell Biol.* 17:489–498. http://dx.doi.org/10.1016/j.ceb.2005.08.013

Sutherland, T.C., P. Quattroni, R.M. Exley, and C.M. Tang. 2010. Transcellular passage of *Neisseria meningitidis* across a polarized respiratory epithelium. *Infect. Immun.* 78:3832–3847. http://dx.doi.org/10.1128/IAI.01377-09

Tilney, L.G., D.J. DeRosier, and M.S. Tilney. 1992. How *Listeria* exploits host cell actin to form its own cytoskeleton. I. Formation of a tail and how that tail might be involved in movement. *J. Cell Biol.* 118:71–81. http://dx.doi.org/10.1083/jcb.118.1.71

van Klinken, B.J., A.W. Einerhand, L.A. Duits, M.K. Makkink, K.M. Tytgat, I.B. Renes, M. Verburg, H.A. Büller, and J. Dekker. 1999. Gastrointestinal expression and partial cDNA cloning of murine Muc2. *Am. J. Physiol.* 276:G115–G124.

Wang, J.A., T.F. Meyer, and T. Rudel. 2008. Cytoskeleton and motor proteins are required for the transcytosis of *Neisseria gonorrhoeae* through polarized epithelial cells. *Int. J. Med. Microbiol.* 298:209–221. http://dx.doi.org/10.1016/j.ijmm.2007.05.004

Watson, R.O., and J.E. Galán. 2008. *Campylobacter jejuni* survives within epithelial cells by avoiding delivery to lysosomes. *PLoS Pathog.* 4:e14. http://dx.doi.org/10.1371/journal.ppat.0040014

Xie, Y., K.J. Kim, and K.S. Kim. 2004. Current concepts on *Escherichia coli* K1 translocation of the blood-brain barrier. *FEMS Immunol. Med. Microbiol.* 42:271–279. http://dx.doi.org/10.1016/j.femsim.2004.09.001

Zhang, J.R., K.E. Mostov, M.E. Lamm, M. Nanno, S. Shimida, M. Ohwaki, and E. Tuomanen. 2000. The polymeric immunoglobulin receptor translocates *pneumococci* across human nasopharyngeal epithelial cells. *Cell.* 102:827–837. http://dx.doi.org/10.1016/S0092-8674(00)00071-4

SUPPLEMENTAL MATERIAL

Nikitas et al., http://www.jem.org/cgi/content/full/jem.20110560/DC1

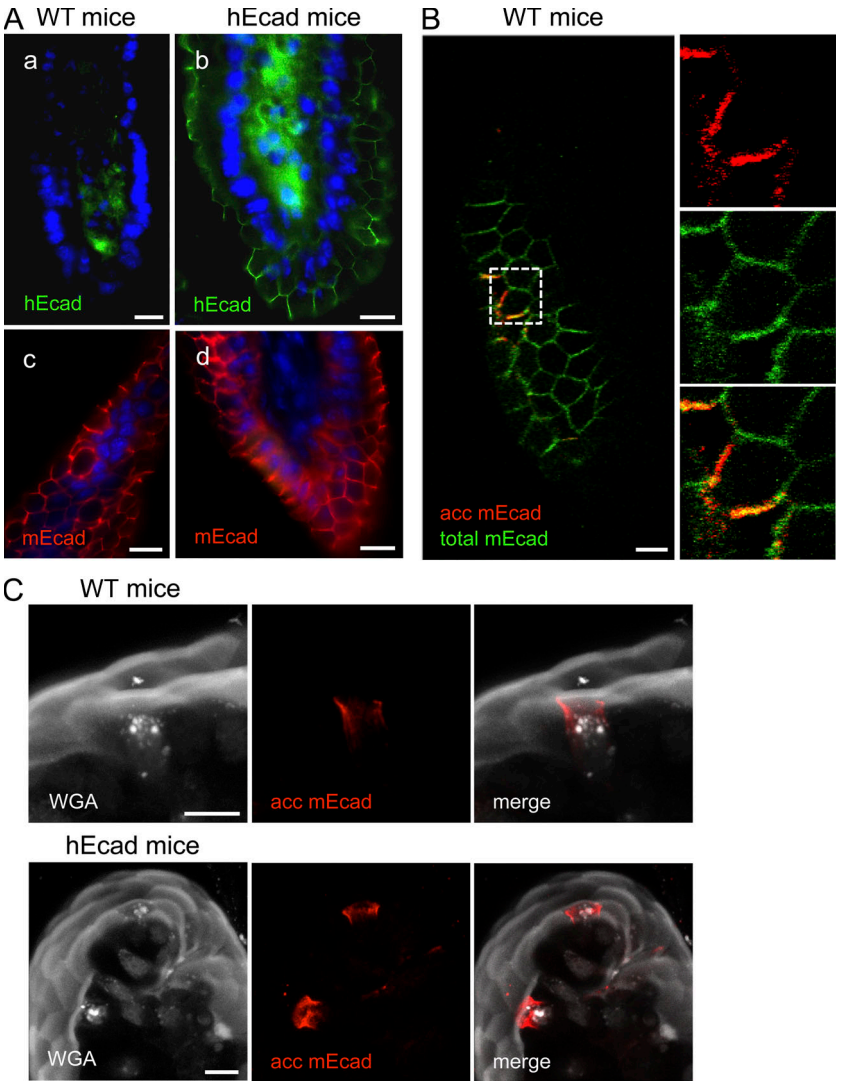

Figure S1. Ecad accessibility is an intrinsic property of intestinal villus epithelium. (A) Frozen 7-µm-thick sections from small intestine of WT (a and c) and *iFABP*-hEcad transgenic mice (b and d) were stained for hEcad (a and b), mEcad (c and d), and nuclei (blue). (a and b) Note that the green signal detected in the lamina propria corresponds to endogenous mouse immunoglobulins stained by the secondary anti–mouse antibody. (B) Accessible (acc) mEcad is detected in WT mice. Optical section of intestinal villus stained for mEcad before (red) and after tissue permeabilization (green). (right) Separated channels and merge of the boxed region, showing accessible mEcad–expressing cells. (C) Accessible mEcad is detected in WT mice similarly to *iFABP*-hEcad transgenic mice around GCs. Stack projection of nonpermeabilized intestinal villi of WT (top) and *iFABP*-hEcad transgenic mouse (bottom) stained with WGA and for accessible mEcad. Pictures are representative of three mice. Bars, 10 µm.

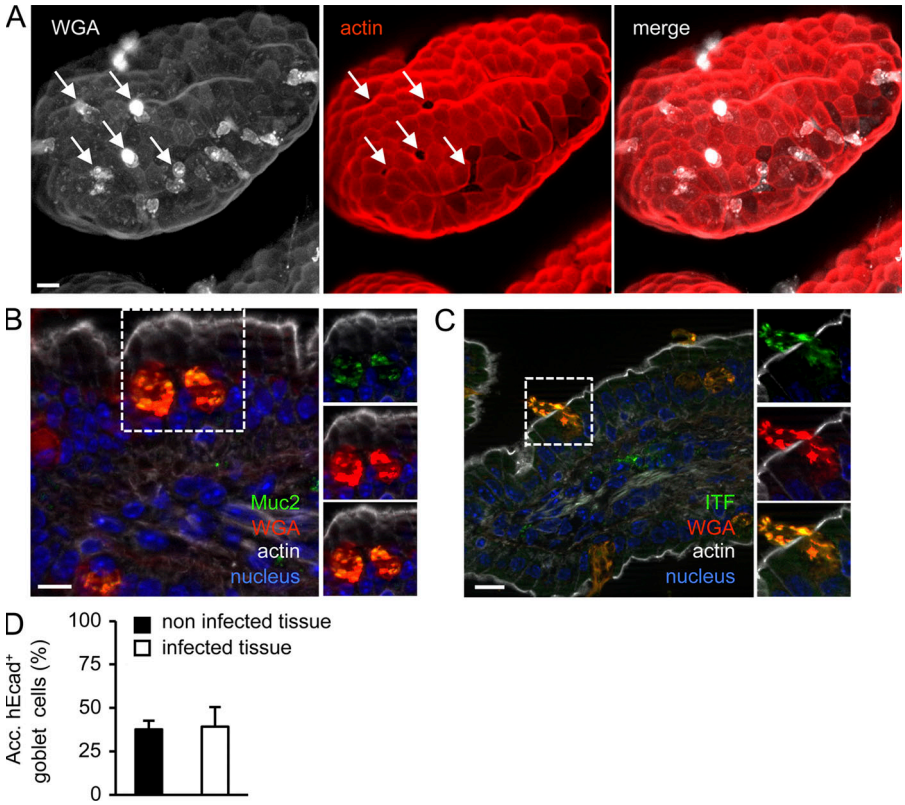

Figure S2. WGA^{hi} cells are GCs that lack apical actin cytoskeleton. (A) WGA^{hi} cells lack an apical actin network (arrows) in contrast to neighboring IECs. Stack projection of whole mount intestinal villus stained with WGA and for F-actin. (B) WGA^{hi} cells are positive for the specific GC marker Muc-2. Thin cryosection of intestinal villus stained with WGA and for Muc-2, F-actin, and nuclei. Lateral panels show separated and merged channels of the boxed region. (C) WGA^{hi} cells are positive for the specific GC marker ITF. Thin cryosection of intestinal villus stained with WGA and for ITF, F-actin, and nuclei. Lateral panels show separated channels and a merge of the boxed region. (A–C) Pictures are representative of three mice. Bars, 10 µm. (D) Quantification of GCs expressing luminally accessible (acc.) hEcad in intestinal villi that are noninfected or are infected with *Lm* for 30 min. Error bars indicate SD. $n = 30$ villi from three mice.

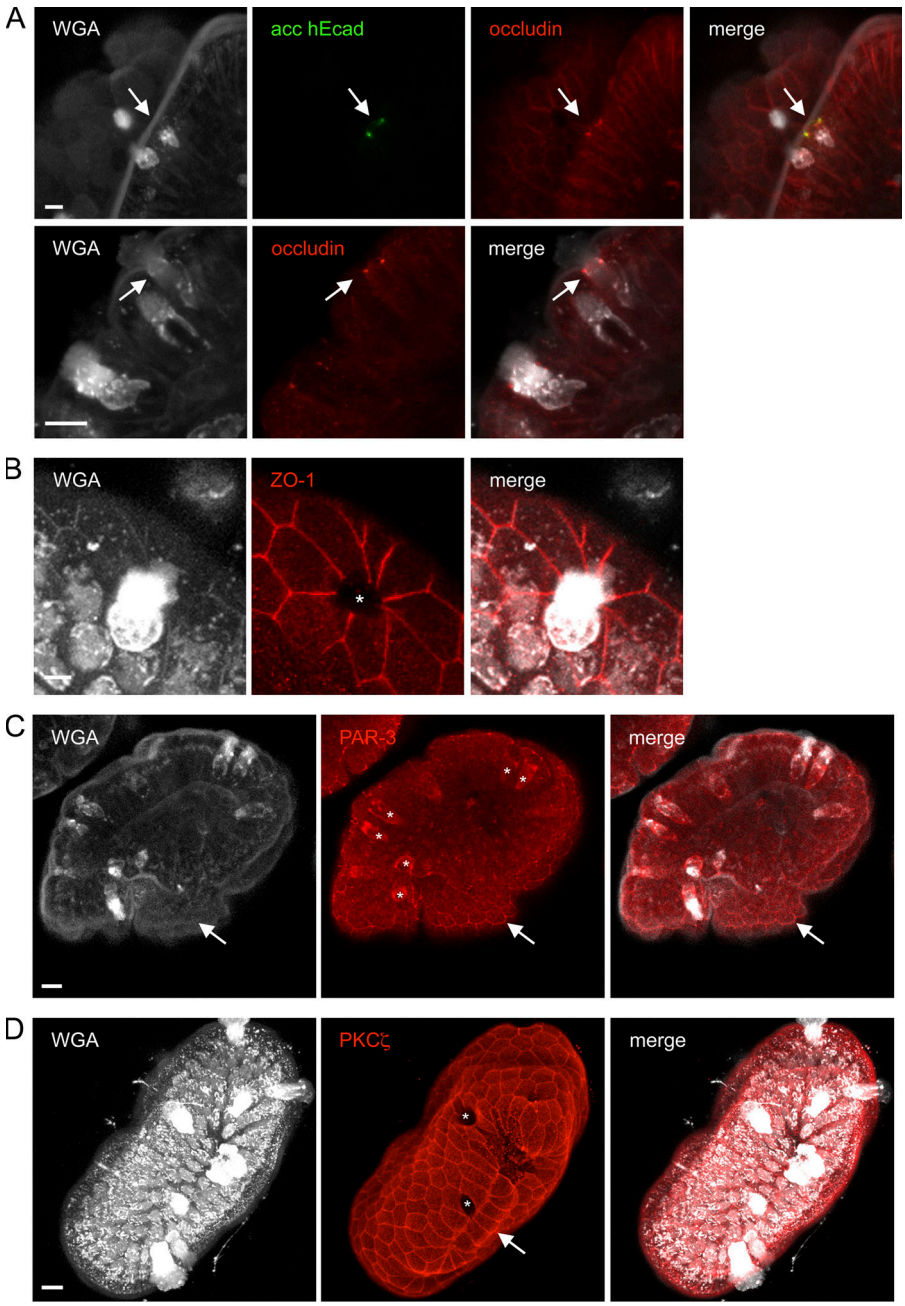

Figure S3. GCs exhibit disorganized TJs. (A) Stack projections of intestinal villi stained with WGA and for accessible (acc) hEcad and occludin. Arrows point to GCs expressing accessible Ecad. (B) Stack projection of intestinal villus stained with WGA and for ZO-1. Asterisks identify a GC. (C) Lower magnification of Fig. 3 C, stack projection of a villus stained with WGA and for PAR-3. Asterisks indicate WGA^{hi} cells with a disorganized PAR-3 expression and localization pattern. Arrows indicate an IEC with normal accumulation of PAR-3 at junctional complexes. (D) Stack projection of an intestinal villus stained with WGA and for PKCζ. Asterisks show GCs, and the arrow indicates an IEC with a normal accumulation of PKCζ at junctional complexes. Pictures are representative of three mice. Bars, 10 µm.

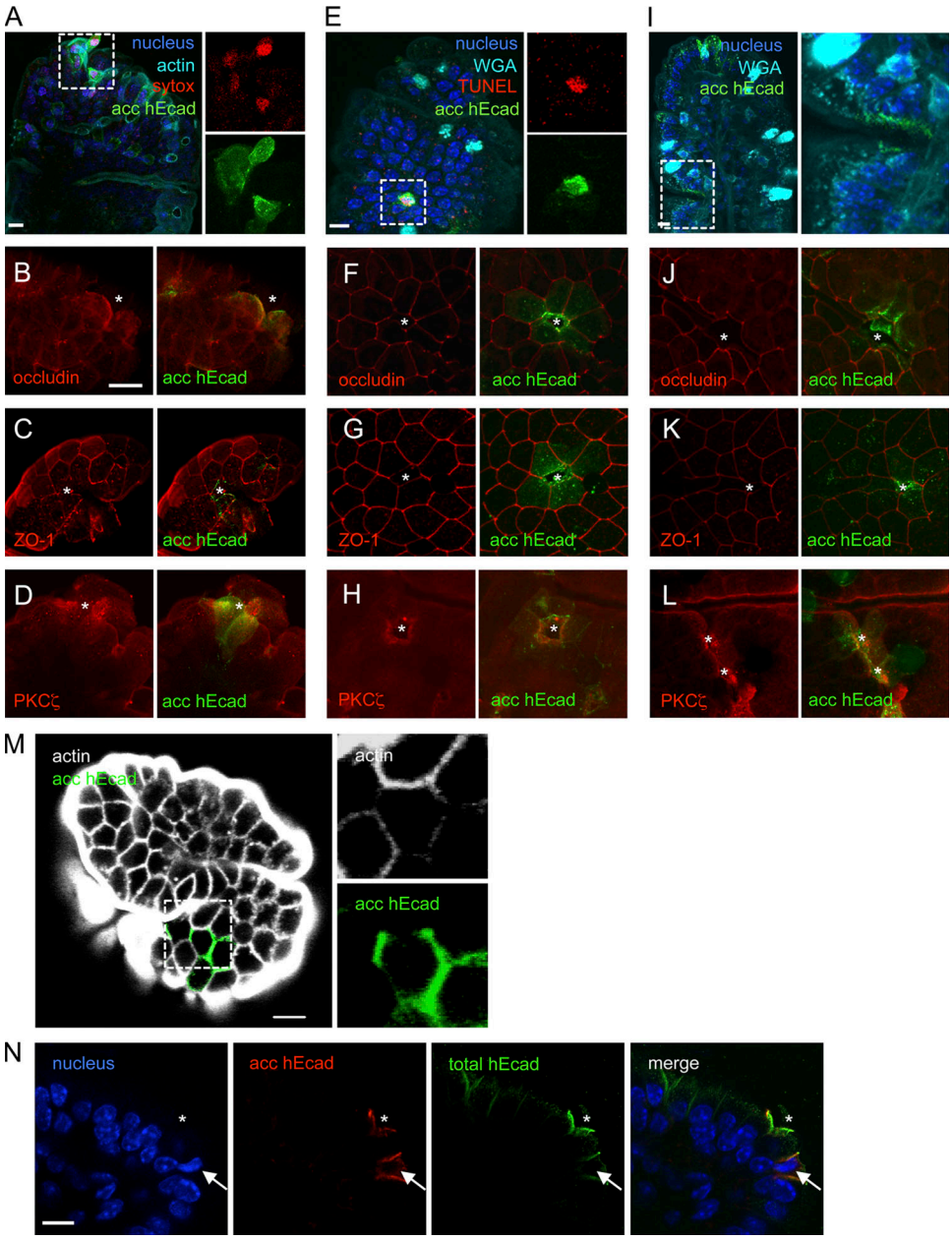

Figure S4. Characterization of non-GC subpopulations expressing luminally accessible Ecad. (A) Accessible (acc) hEcad is present on the villus tip at an apoptotic cell extrusion site visualized with Sytox labeling and stained for F-actin and nuclei. Lateral panels show separated channels of the boxed region. (B and C) Occludin and ZO-1 are delocalized at the villus tip (asterisks) where hEcad is accessible. (D) PKCζ is enriched at the tip of the villus (asterisks) where hEcad is accessible. (E) Apoptotic cell extrusion sites are present at the lateral side of intestinal villus as depicted by the TUNEL staining and show accessible hEcad. Lateral panels show separated channels of the boxed region. (F–H) TJ proteins occludin and ZO-1 are mislocalized at sites of cell extrusion at the lateral side of intestinal villus (asterisks) where hEcad is accessible, whereas PKCζ is increased. (I) Accessible hEcad is present in villus epithelial folds. Lateral panels show magnification of the boxed region. (J–L) TJ proteins occludin and ZO-1 are mislocalized where hEcad is accessible in villus epithelial folds (asterisks), whereas PKCζ is increased. (A–L) 150-µm-thick vibratome sections are shown. (M) Optical section of an intestinal villus stained for F-actin and luminally accessible hEcad, showing a cell expressing accessible hEcad and lacking cortical F-actin at these sites. The boxed area is shown at higher magnification on the right. (N) Optical section of one villus showing an extruded (asterisks) and extruding cell (arrows) with accessible hEcad and enrichment of total hEcad. (M and N) Whole mount tissues are shown. (A–N) Pictures are representative of three mice. Bars, 10 µm.

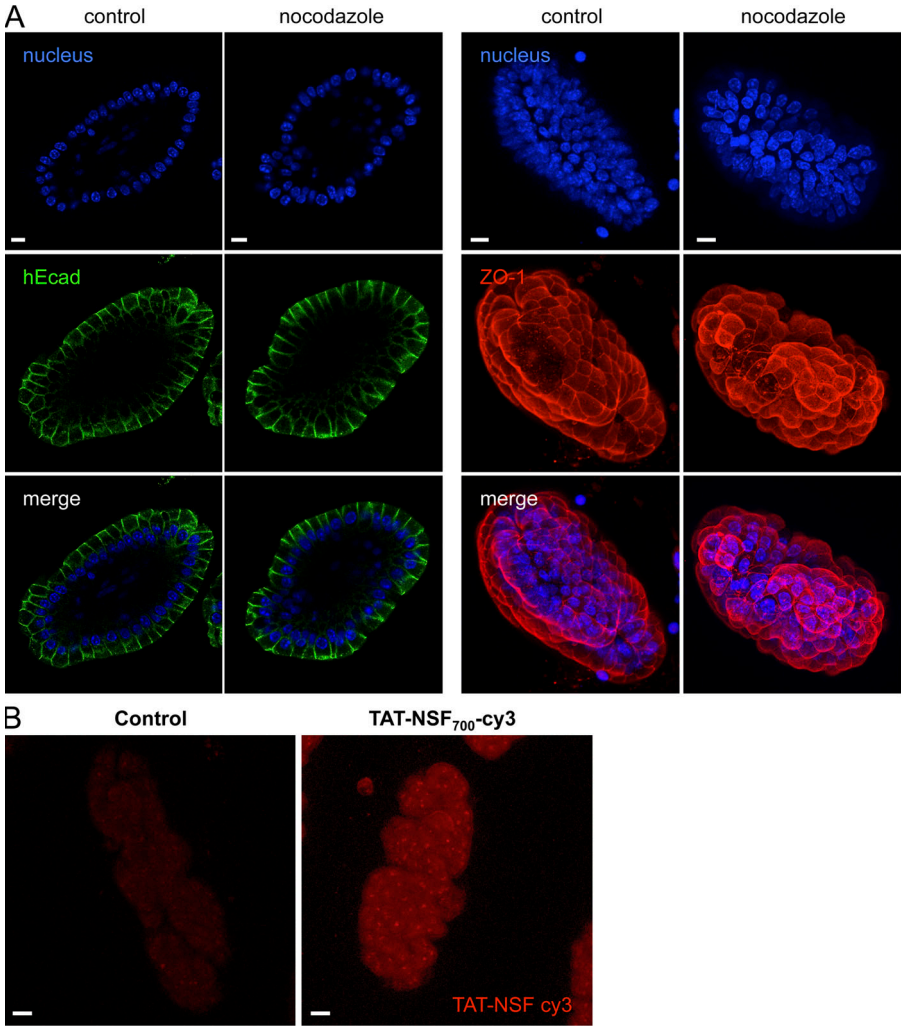

Figure S5. Nocodazole treatment does not affect adherens junction and TJ integrity. (A) Left panels show optical sections of an intestinal villus treated or not with nocodazole and stained for nucleus and hEcad. Right panels show stack projections of intestinal villus treated or not with nocodazole and stained for nucleus and ZO-1. Pictures are representative of three mice. (B) TAT-NSF_{700}–cy3 enters in the intestinal epithelium. Stack projection of an intestinal villus treated with TAT-NSF_{700}–cy3 (right) for 30 min compared with a nontreated tissue (left). Pictures are representative of two mice. Bars, 10 µm.

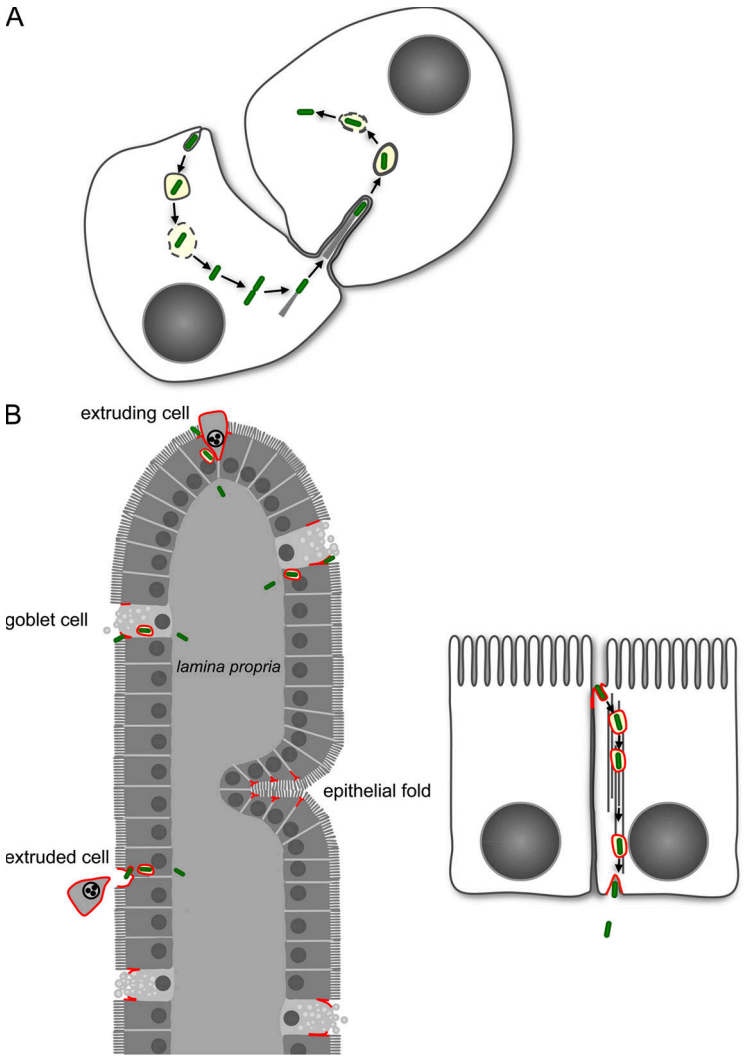

Figure S6. *Lm* cell infectious process. (A) Classical *Lm* in vitro cell infectious cycle, as described initially by Tilney and Portnoy (1989). After internalization into cells, *Lm* (green) resides in a vacuole from which it escapes as a result of the activity of the pore-forming toxin LLO. Once in the cytoplasm, *Lm* replicates and is propelled by ActA-dependent actin polymerization and spreads to neighboring cells. (B, left) Schematic representation of *Lm* invasion of the intestinal villus epithelium in vivo. *Lm* (green) enters IECs by interacting with luminally accessible Ecad (red), observed at cell–cell junctions between GCs and adjacent enterocytes, around extruding enterocytes at the tip, and lateral sides of villi, as well as at cell–cell junctions between enterocytes located in villus epithelial folds. (right) Schematic representation of *Lm* transcytosis across the intestinal epithelium. *Lm* (green) interacts with luminally accessible Ecad (red) and is internalized. After entry, the *Lm*-containing vacuole is rapidly translocated in a microtubule-dependent manner to the basolateral pole of the cell where it is exocytosed, releasing *Lm* subepithelially.

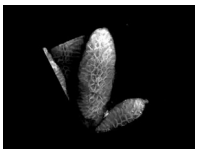

Video 1. Three-dimensional reconstruction of an intestinal villus. This video is related to Fig. 1 A. Ecad expression in intestinal villi. Whole mount intestinal tissue was stained for total hEcad (white) after permeabilization, and images were acquired as a z stack by two-photon microscopy and assembled as a three-dimensional reconstruction with Imaris software.

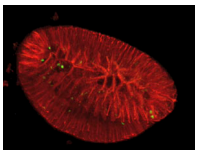

Video 2. Three-dimensional reconstruction of an intestinal villus invaded by *Lm*. This video is related to Fig. 1 B. Ligated intestinal loops were infected by *Lm* for 30 min, fixed, and stained for total hEcad (red) and *Lm* (green) after permeabilization. Images of whole mount tissue were acquired as a z stack by two-photon microscopy and assembled as a three-dimensional reconstruction with Imaris software.

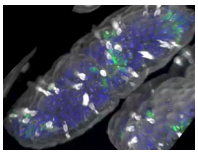

Video 3. Intestinal cells express luminally accessible Ecad. This video is related to Fig. 2. Whole mount intestinal tissue was stained before permeabilization with WGA (white) and for accessible hEcad (green) and after permeabilization for nuclei (blue). Villus is oriented with the villus tip facing the viewer. Images were acquired as a z stack by confocal microscopy and assembled as a three-dimensional reconstruction with Imaris software.

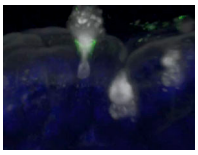

Video 4. Luminally accessible Ecad around GCs. This video is related to Figs. 2 and 3. Whole mount tissue was stained as described for Video 3. The video shows one GC surrounded by accessible Ecad (green) and expelling its mucus content (white). Images were acquired and assembled as described for Video 3.

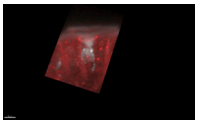

Video 5. Redistribution of occludin around GCs. This video is related to Fig. 3 B. Whole mount intestinal tissue was stained for occludin (red) and with WGA (white). The video shows one GC with its mucus content presenting more occludin at the junctional complex compared with its neighboring cells. Images were acquired and assembled as described for Video 3.

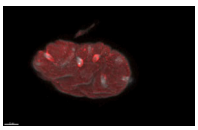

Video 6. Depolarization of PAR-3 around GCs. This video is related to Fig. 3 C. Whole mount intestinal tissue was stained for PAR-3 (red) and with WGA (white). The video shows GCs (white) with depolarized PAR-3 while PAR-3 is accumulated at the junctional complexes on enterocytes. Images were acquired and assembled as described for Video 3.

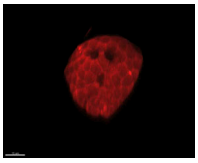

Video 7. Depolarization of PKCζ around GCs. This video is related to Fig. 3 C. Whole mount intestinal tissue was stained for PKCζ, and images were acquired and assembled as described for Video 3.

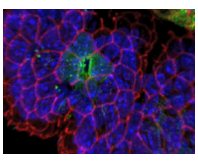

Video 8. Luminally accessible Ecad at sites of cell extrusion. This video is related to Fig. S4. A vibratome section of an intestinal villus was stained before permeabilization for accessible hEcad (green) and after permeabilization for ZO-1 (red) and nuclei (blue). The video shows a gap after cell extrusion surrounded by accessible Ecad on the lateral side of an intestinal villus. Images were acquired and assembled as described for Video 3.

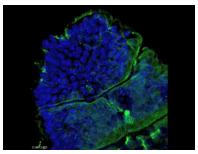

Video 9. Luminally accessible Ecad within villus epithelial folds. This video is related to Fig. S4. (first) Vibratome section of intestinal villus was stained for PKCζ (aPKC; green) and nuclei (blue). The video shows an intestinal villus with villus epithelial folds. (second) Vibratome section of intestinal villus was stained as described in Video 3. The video shows a villus epithelial fold with accessible Ecad (green). Images were acquired and assembled as described for Video 3.

Table S1. Overview of TJ characteristics around cells expressing luminally accessible Ecad

Junction marker	Junctions around accessible Ecad⁺ GCs	Junctions around accessible Ecad⁺ extruding cells		Junctions within accessible Ecad⁺ villus folds
		Villus tip	Villus lateral side	
occludin	thickened	apically enriched dislocalized	mislocalized	mislocalized
ZO-1	mislocalized	mislocalized	mislocalized	mislocalized
PKCζ	mislocalized	enriched	enriched	enriched
PAR-3	delocalized	unremarkable	unremarkable	unremarkable

This table is related to Fig. 3 and Fig. S4.

REFERENCE

Tilney, L.G., and D.A. Portnoy. 1989. Actin filaments and the growth, movement, and spread of the intracellular bacterial parasite, *Listeria monocytogenes*. *J. Cell Biol.* 109:1597–1608. http://dx.doi.org/10.1083/jcb.109.4.1597